APPROXIMATE BAYESIAN COMPUTATION FOR PROBABILISTIC DECLINE CURVE ANALYSIS IN UNCONVENTIONAL RESERVOIRS

By

Mohit Paryani

RECOMMENDED:

Dr. Mohabbat Ahmadi
Advisory Committee Chair

Dr. Catherine Hanks
Advisory Committee Co-Chair

Dr. Obadare Awoleke
Advisory Committee Member

Dr. Abhijit Dandekar,
Chair, Department of Petroleum Engineering

APPROVED:

Dr. Douglas Goering
Dean, College of Engineering and Mines

Dr. John Eichelberger
Dean of the Graduate School

26 October 2015

Date

APPROXIMATE BAYESIAN COMPUTATION FOR PROBABILISTIC DECLINE CURVE ANALYSIS IN UNCONVENTIONAL RESERVOIRS

A

THESIS

Presented to the Faculty

of the University of Alaska Fairbanks

in Partial Fulfillment of the Requirements

for the Degree of

MASTER OF SCIENCE

By

Mohit Paryani, B.E.

Fairbanks, Alaska

December 2015

Abstract

Predicting the production rate and ultimate production of shale resource plays is critical in order to determine if development is economical. In the absence of production from the Shublik Shale, Alaska, Arps' decline model and other newly proposed decline models were used to analyze production data from oil producing wells in the Eagle Ford Shale, Texas. It was found that shales violated assumptions used in Arps' model for conventional hydrocarbon accumulations. Newly proposed models fit the past production data to varying degrees, with the Logistic Growth Analysis (LGA) and Power Law Exponential (PLE) models making the most conservative predictions and those of Duong's model falling in between LGA and PLE. Using a regression coefficient cutoff of 95%, we see that the LGA model fits the production data (both rate and cumulative) from 81 of the 100 wells analyzed. Arps' hyperbolic and the LGA equation provided the most optimistic and pessimistic reserve estimates, respectively.

The second part of this study investigates how the choice of residual function affects the estimation of model parameters and consequent remaining well life and reserves. Results suggest that using logarithmic rate residuals maximized the likelihood of Arps' equation having bounded estimates of reserves. We saw that approximately 75% of the well histories that were fitted using the logarithmic rate residual had hyperbolic b-values < 1, as opposed to 40% using the least squares error function—an 87.5% increase. This is because they allow the most recent production data to be weighted more heavily, thereby ensuring that the fitted parameters reflect the current flow regime in the drainage area of the wells.

In the third part of this work, in order to quantify the uncertainty associated with Decline Curve Analysis (DCA) models, a methodology was developed that integrated DCA models with an approximate Bayesian probabilistic method based on rejection sampling. The proposed Bayesian model was tested by history matching the simulation results with the observed production data of 100 gas wells from the Barnett Shale and 21 oil wells from the Eagle Ford Shale. For example, in Karnes County, the ABC P90-P50-P10 average interval per well was 170-184-204 MSTB, while the true average cumulative production per well was 183 MSTB. The ABC methodology coupled with any deterministic DCA model will help in long-term planning of operations necessary for optimal/effective field development.

Dedicated to

my mother for her unconditional love, support & motivation

Table of Contents

List of Figures

List of Tables

Acknowledgments

I would like to express my sincere gratitude to my advisor Dr. Mohabbat Ahmadi for his guidance, support, and confidence in my research and graduate studies. I would also like to thank my advisory committee, Dr. Obadare Awoleke and Dr. Catherine Hanks, for their invaluable inputs and commitment towards my research. I am thankful to Dr. Ron Barry for helping me with statistics from time to time.

I am grateful to the Petroleum Engineering Department Chair Dr. Abhijit Dandekar, the Dean of the Graduate School Dr. John Eichelberger, and the Alaska Department of Natural Resources for funding my research and graduate studies.

I would also like to thank my parents, Mr. Ramchand Paryani and Mrs. Bharti Paryani, and my sisters for their unconditional love and support. Last of all, I am thankful to my friends for their support during my stay at UAF.

Chapter 1. Introduction

The development of the Eagle Ford Shale and other analogous shale intervals indicates that a good understanding of both the geology and the response of the shale to stimulation are critical for effective and economic production. As these unconventional plays have been developed, it has become clear that traditional Arps' models are inadequate to analyze previous production history profiles and predict future well performance of shale resource plays.

The development of the Shublik Shale as a resource play is hampered by the lack of this type of production performance information. Production data from a close geologic analogue, the Eagle Ford Shale, was used to develop a better understanding of what critical data need to be collected from the Shublik to adequately model and predict potential production from a Shublik well. Data from the Eagle Ford is augmented with Shublik data where such data are publicly available. Decline curve analysis (DCA) is a technique where production data from a well or reservoir is used to predict the well/reservoir's future production. Two important goals of DCA are to estimate the remaining reserves and the remaining life down to a specified economic limit.

Wells producing from shale reservoirs are all hydraulically fractured. Production commences with 100% water and the water cut decreases over the life of the well. It takes a few weeks to a few months for the oil/gas production rate to reach its maximum, followed by a steep decline in production. This is partially due to production being dominated by fractures in the stimulated reservoir volume (SRV) with little contribution from the reservoir matrix (Chaudhary et al., 2011). This and other complexities of shale reservoirs cause Arps' model to overestimate reserves, often yielding mathematically infinite reserve estimates due to fitting production/time data with $b>1$. To address this problem, different decline curve analysis models have been proposed for tight shale reservoirs, such as Power Law Exponential (PLE), Duong's model, and Logistic Growth Analyses (LGA).

1.1 Evaluating DCA models in Eagle Ford Shale wells--data and methodology

The Eagle Ford Shale play, located in the Maverick Basin of Southeast Texas, is approximately 400 miles long and 50 miles wide (Figure 1.1; Chaudhary et al., 2011). In this study, production data of a hundred oil wells in the Eagle Ford Shale play was obtained from the Texas Rail Road

Commission (TRRC) website. The hundred wells covered eight counties, namely, Burleson, De Witt, Dimmit, Gonzales, Karnes, La Salle, Live Oak, and Zavala (Figure 1.1). Some, but not all, of the wells' horizontal length and number of fracture stages were reported.

The main objective behind analyzing this data is to check the applicability of the existing decline curve models on Eagle Ford Shale wells. The general procedure is to tune the existing decline models by matching the production rate and/or cumulative data of each well. A model is said to fit fairly well when the regression coefficient between the model output and the actual production date is greater than or equal to 95%. Each tuned model is then used to predict future production rates, remaining reserves, and remaining time to reach the abandonment rate of 2 STB/day for each well. The length of production history varies from 15 to 48 months for different wells.

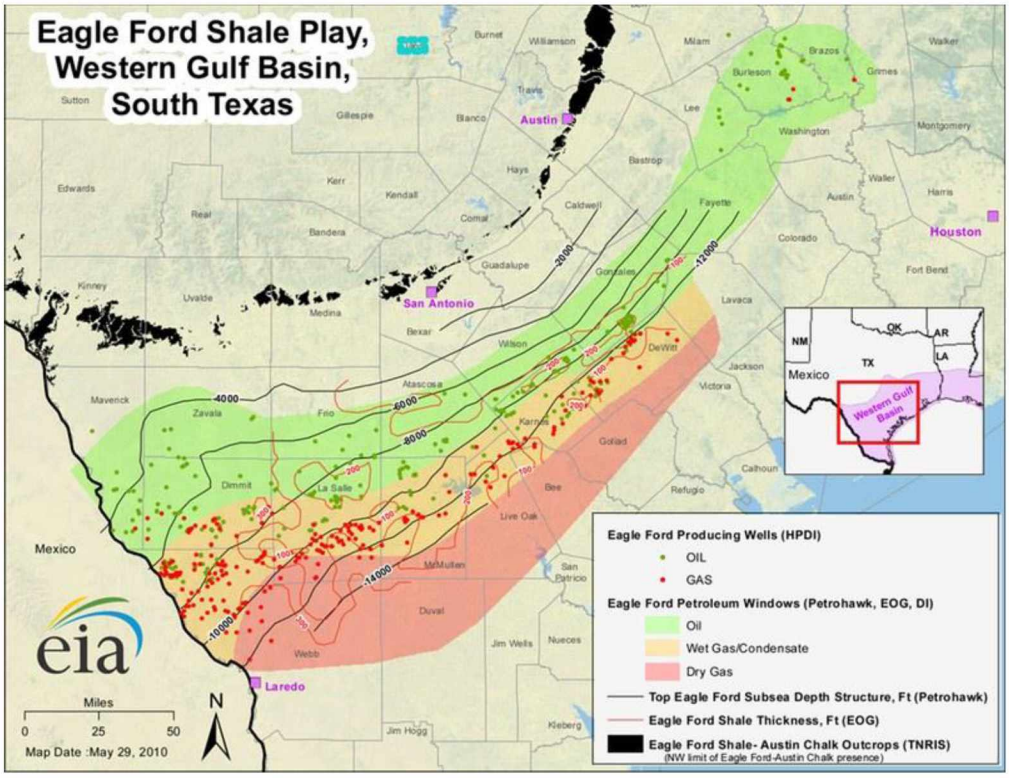

Figure 1.1: Map of Eagle Ford shale (DuBose, 2011)

1.2 Incorporating uncertainty in DCA modeling of Shale wells

Reserve estimates and production forecasts in hydraulically fractured shale wells have considerable uncertainty. One major source of uncertainty in the forecasts arises from the interaction between the induced hydraulic and natural fractures. This results in some wells having

a variable Stimulated Reservoir Volume (SRV). The variable SRV causes the well to deplete in different stages, which increases the uncertainty. The first depletion stage from the highly conductive fractures explains the early high production rates. This is followed by production from the moderate and finally low conductivity fractures, respectively. In other words, the more conductive SRV depletes first (Suliman et al., 2013). Other sources of uncertainty include lack of long term production history, complex flow geometry, and variability in completion properties (Agrawal et al., 2012).

Numerous deterministic DCA models have been established to analyze production data from hydraulically fractured shale wells. However, none of these models quantify the uncertainty in production forecasts (Dossary and McVay, 2012). Probabilistic DCA models that do quantify uncertainty in the forecasts have been proposed; however, these models are either not tested with enough wells to be well calibrated or very complicated to apply.

1.3 Objectives

The objective of the first part of this study is to compare forecasts of these four decline models when applied to hydraulically fractured horizontal shale oil wells. Production data from 100 oil wells from eight counties in the Eagle Ford Shale play of southeast Texas were analyzed as part of this work. Using a regression coefficient cutoff of 95%, we see that the LGA model fits the production data (both rate and cumulative) from 81 of the 100 wells analyzed. Arps' hyperbolic and the LGA equation provided the most optimistic and pessimistic reserve estimates, respectively.

The second part of this work investigated how the choice of residual function affects the estimate of model parameters and consequent remaining well life and reserves. The objective was to develop a methodology that maximizes the likelihood of satisfactorily fitting the data with a b-value < 1 without developing complicated routines. We explored the use of different residual functions and found out that using logarithmic rate residuals maximized this likelihood. We saw that approximately 75% of the well histories that were fitted using the logarithmic rate residual had hyperbolic b-values < 1, as opposed to 40% using the least squares error function—an 87.5% increase.

The objective of the third part of this study is to develop a Bayesian methodology that can reliably quantify the uncertainty in the production forecasts regardless of the stage of depletion. The advantage of the proposed probabilistic DCA model is that it relies solely on the analysis of the production data.

Chapter 2. Decline Curve Analysis and its Application to Eagle Ford Production Data

2.1 Introduction

Predicting the future production behavior of unconventional reservoirs is critical for determining the economic viability of a shale resource play. However, existing DCA techniques assume: a) constant bottomhole pressure; b) boundary dominated flow; c) unchanging drainage area; and d) constant skin factor. Conventional reservoirs usually have a short transient phase followed by boundary dominated flow. In transient flow, the pressure pulse is moving away from the wellbore; hence, the reservoir acts infinite. The time when the pressure pulse reaches a flow boundary such as a fault or pay zone pinch out is inversely proportional to the permeability of the reservoir. Conventional reservoirs hit boundary dominated flow a few days after the start of production. However, in the case of shale reservoirs, it is uncertain if the flow will become boundary dominated during its producing life due to extremely low permeability. This and other complexities of shale reservoirs cause the b value for Arps' hyperbolic decline equation to become greater than 1 (Arps, 1945; Lee and Sidle, 2010).

Thus, the behavior of fluid flow in extremely tight porous media neighbored by high-conductivity induced and/or natural fractures creates challenges in forecasting the performance of shale oil wells and reservoirs. Transient and fracture-dominated flow regimes in shale reservoirs demand new well performance evaluation techniques. Evaluating Arps' model assumptions for decline curve analysis highlights its limitations when applied to shale reservoirs and the need for better models for these unconventional reservoirs. This chapter discusses the application of different decline curve analysis models that have been proposed for tight shale reservoirs, such as Power Law Exponential (PLE), Duong's model, and Logistic Growth Analyses (LGA), to Eagle Ford production data.

2.2 Production data analysis

Figure 2.1 and Figure 2.2 show the average first year production rate of wells in Karnes and Zavala counties versus horizontal length and fracturing stages, respectively. Despite the slightly upward trend shown, there is no strong correlation between rate and completion parameters. The lack of

correlation indicates that the reservoir is heterogeneous. If the reservoir were homogeneous, the rates would increase proportionally with completion parameters (Chaudhary et al., 2011).

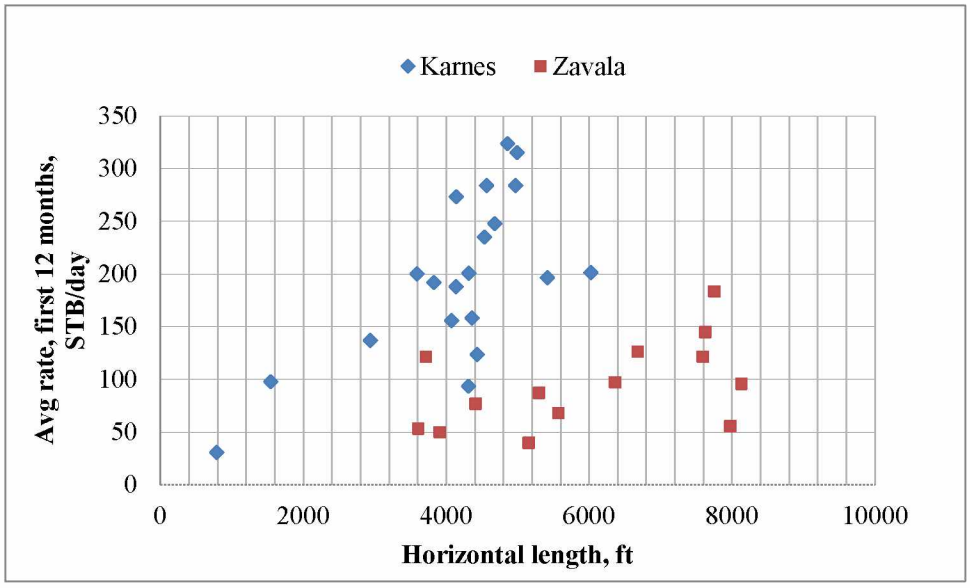

Figure 2.1: Effect of horizontal length on average rate

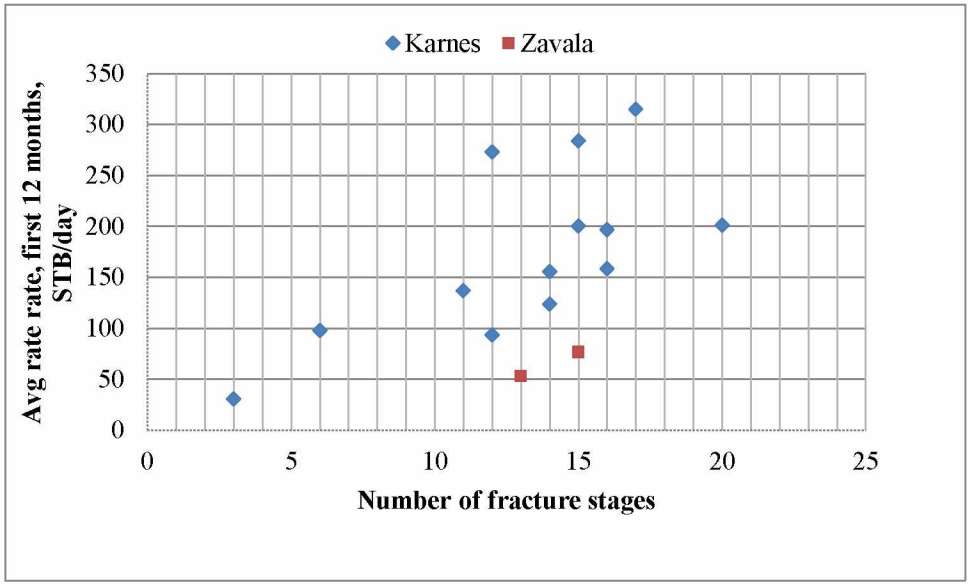

Figure 2.2: Effect of number of fracture stage on average rate, first 12 months

Figure 2.3 shows an example of a log-log diagnostic plot of rate versus time. The objective of this plot is to identify flow regimes. A slope of -0.5 in the plot's trend line implies that the flow regime is linear. A slope of -1 during the later stages of production implies that the well has reached

boundary conditions and that the flow regime is now boundary-dominated. A slope of -0.25 during the early stages of production implies that linear flow is preceded by a bilinear flow regime (Kanfar and Wattenbarger, 2012). In Figure 2.3, the slopes of the two trend lines are -0.5 and -1 based on the angles made by the two trendlines with the x-axis, indicating that the well has felt its boundary.

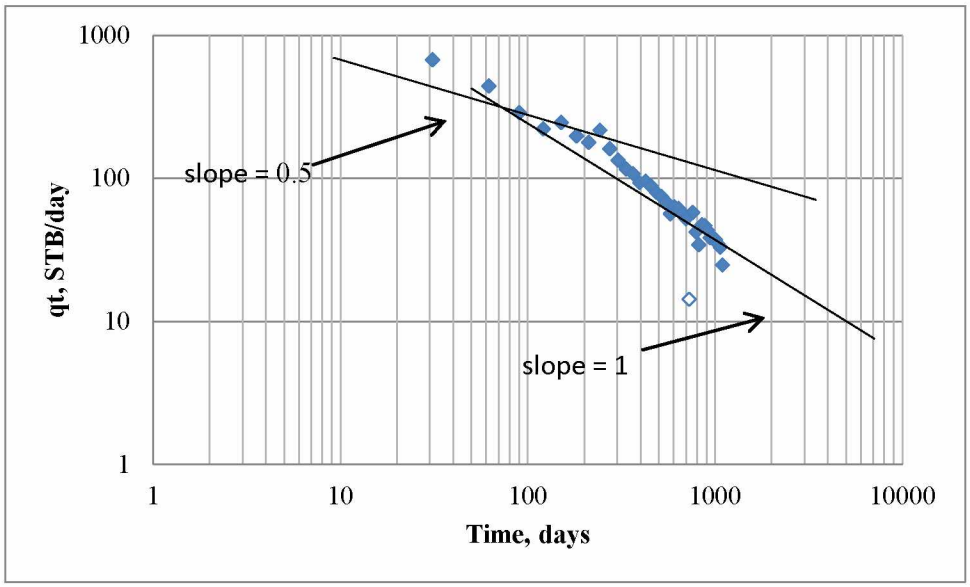

Figure 2.3: Diagnostic log-log plot of rate vs. time to identify flow regimes

2.3 Arps' decline curve model

Arps (1945) observed that the ratio of production rate to change in production rate played a crucial role in determining the type of decline a well would undergo. The exponential form of Arps' decline model (b=0) typically applies to conventional reservoirs with reasonably high permeability in which a short transient phase is usually followed by boundary dominated flow. However, in the case of shale reservoirs where matrix permeability is extremely low, it is uncertain and probably unlikely that flow will become boundary-dominated during a typical well's producing life (Arps, 1945; Lee and Sidle, 2010).

The hyperbolic form of Arps' model (0<b<1) is typically a concave up curve on a semi-log plot of rate versus time. This model is frequently used for conventional reservoirs. However, in cases where boundary dominated flow has been reached, it can also be used for low permeability reservoirs. As stated previously, shale reservoirs have extremely low permeability in the range of

nano-darcies. The nano-darcy matrix permeability coupled with the high permeability hydraulic fracture is the cause of long transient flow in shale reservoirs. These wells exhibit high initial rates followed by rapid declines. This and other complexities of shale reservoirs can cause the b-value for Arps' hyperbolic to be greater than 1 (Urbancic and Baig, 2004; Lee and Sidle, 2010).

The use of Arps' model to analyze production data from shale reservoirs is not recommended because these reservoirs sometimes do not attain boundary-dominated flow due to their low permeability. Moreover, the drainage area is not constant because the pressure pulse continues to propagate from near the wellbore/fracture to other areas of the stimulated reservoir volume. Under these conditions, the b-value obtained from regression by minimizing the least square error between the values predicted by Arps's hyperbolic model and the actual production data will be greater than 1. This in turn leads to erroneous estimates of reserves. Despite the obvious drawbacks to using Arps' equation in shale reservoirs, it is still a very popular model. We think that this is because (1) it provides a reasonable history match even when b>1 and (2) it is familiar and has a simple form.

In order to compare the impact of different residual functions on b-value estimates, Excel's multivariable solver tool was used to calculate the parameters from Arps' model for different error functions. We estimated the decline rate D_i, initial production rate q_i, and the decline exponent b. This was done by fitting the production data/history using least residual squares. We will discuss the improvements obtained by using different residual functions later in this thesis. Once the parameters were obtained, the estimated ultimate recovery (EUR) and the remaining time to reach abandonment were calculated. This was repeated for 100 wells randomly selected from 8 different counties. Figure 2.4 shows an example history match of Cannon well in Karnes County with Arps' hyperbolic model. In general, it was observed that Arps' hyperbolic model matched well for all the wells, regardless of whether the hyperbolic exponent was normal or abnormal. The significance of the abnormal exponent was felt in high predicted values for remaining life and reserves.

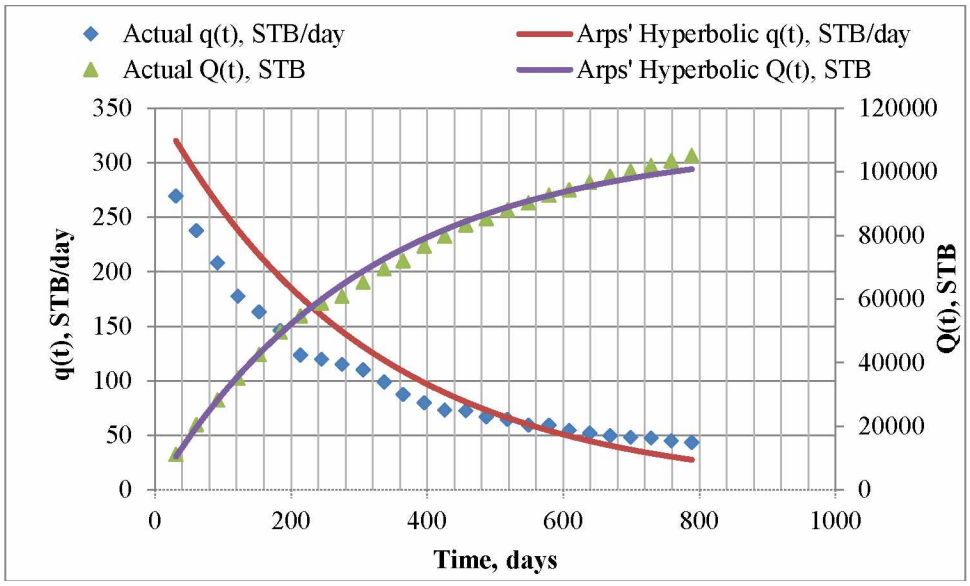

Figure 2.4: Arps' hyperbolic fit for Cannon well (Karnes County) showing rate and cumulative production history match

2.4 Logistic growth analysis

The LGA model (Tsoularis and Wallace, 2001; Clark et al., 2011) is proposed to estimate remaining reserves for reservoirs with extremely low permeability. It was derived from the hyperbolic family of curves and its prediction of cumulative production takes the following form, equation (1):

$$Q(t) = \frac{Kt^n}{a'' + t^n} \tag{1}$$

where 'k' is the carrying capacity or the maximum recoverable oil from the reservoir/well, a'' is a constant, t^n is the time at which half of the recoverable oil has been produced, and 'n' is the hyperbolic exponent.

By differentiating equation (1), the rate form of the LGA model is obtained, as stated below—equation (2):

$$q(t) = n\left(\frac{K}{a}\right)^{\frac{1}{n}} Q(t)^{1-\frac{1}{n}} \left(1 - \frac{Q(t)}{K}\right)^{1+\frac{1}{n}} \tag{2}$$

One of the assumptions of the LGA model is that the parameter k or the recoverable reserves is already known ahead of time, usually by volumetric calculations. However, k can also be a fitting parameter. Another assumption is that a single well will be sufficient to drain the entire reservoir over a long period of time (Clark et al., 2011). The two major advantages of the LGA model are: (1) the form of the equation ensures the reserves estimate is constrained to parameter k (in contrast to Arps' hyperbolic model) and (2) the production rate is eventually terminated at infinite time, which also ensures the reserves estimate is constrained (Clark et al., 2011).

The parameters k, a'', and n were estimated using Excel's multivariable solver tool. The Logistic Growth Analysis model fitted the hundred wells' past production data very well. For the wells with an abnormal hyperbolic exponent, b>1, the LGA model constrained the expected ultimate recovery and reported more realistic results compared to the highly optimistic estimates from the hyperbolic model. Figure 2.5 shows an example history match from Berry well in Karnes County. A very good match for production rate and cumulative production is obtained in this example.

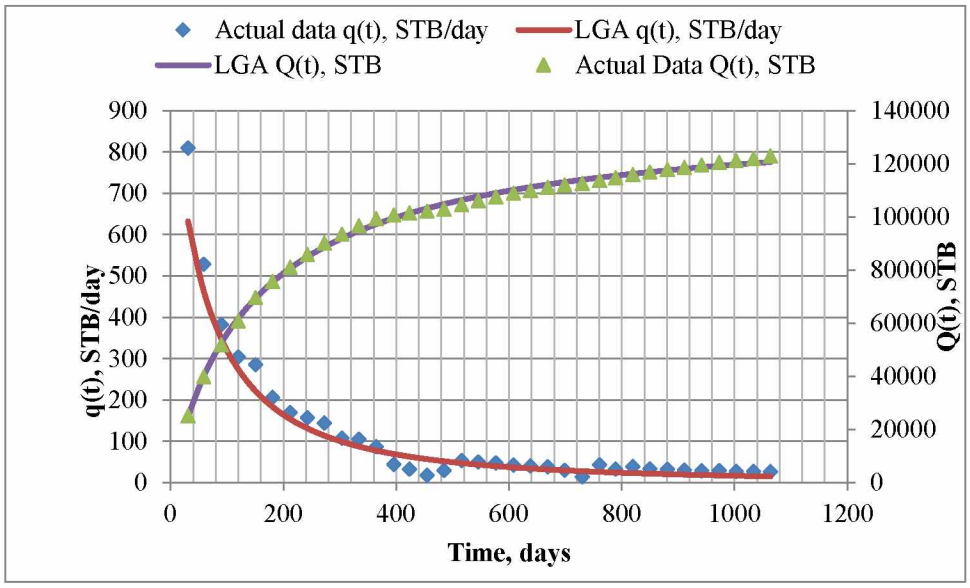

Figure 2.5: Example of good LGA fit for the Berry well

2.5 Duong's model

Duong (2011) observed that a log-log plot of production rate over cumulative production versus time was always a straight line for wells in unconventional reservoirs. The parameters (slope, m and intercept, a) obtained from this plot are the characteristics of the reservoir rock and fracture

stimulation completions. Instead of Arps' model, Duong suggested using the constraints of initial production rate and the production rate at infinity to evaluate rate and cumulative production based on boundary-dominated flow. Duong's work is described primarily by equations (3) and (4):

$$\frac{q(t)}{Q(t)} = at^{-m} \tag{3}$$

$$q(t) = q_1 t(a,m) + q_\infty \tag{4}$$

where $t(a,m) = t^{-m}\exp\left(\left(\frac{a}{1-m}\right)\left(t^{1-m}-1\right)\right)$.

Typical ranges of these parameters are $1 < m < 2$ and $1 < a < 2$. The two major limitations of this model are that when the well is shut in for long periods of time, proper rate initialization according to pressure is required to obtain correct values of parameters a and m. Secondly, in the case of water breakthrough, there is a sudden decrease in the decline rate, which causes an increase in the values of a and m (Duong, 2011).

In order to analyze Eagle Ford production data using Duong's model, two diagnostic plots were generated using equations (3) and (4): log-log plots of $\frac{q(t)}{Q(t)}$ versus time and rate versus $t(a,m)$. By plotting the ratio of rate to cumulative production vs. time, the parameters a and m were obtained. Thereafter, by plotting rate versus the time function, we get parameters q_1 and q_∞. After obtaining all the model parameters, equations (3) and (4) were algebraically manipulated to predict rate and cumulative production (Figure 2.8). Figure 2.6 and Figure 2.7 show example diagnostic plots for Duong's model. Figure 2.6 is a log-log plot of $\frac{q(t)}{Q(t)}$ vs. time. The least square regression trendline tool in Excel gives the values of parameters a and m. Figure 2.7 is a diagnostic plot of rate vs. time, which depends on parameters a and m. The least square regression trendline gives the values of q_1 and q_∞. Note that when the trendline passes through the origin, the value of q_∞ becomes zero, as it is the intercept of the trendline. Figure 2.8 shows a match for Duong's model.

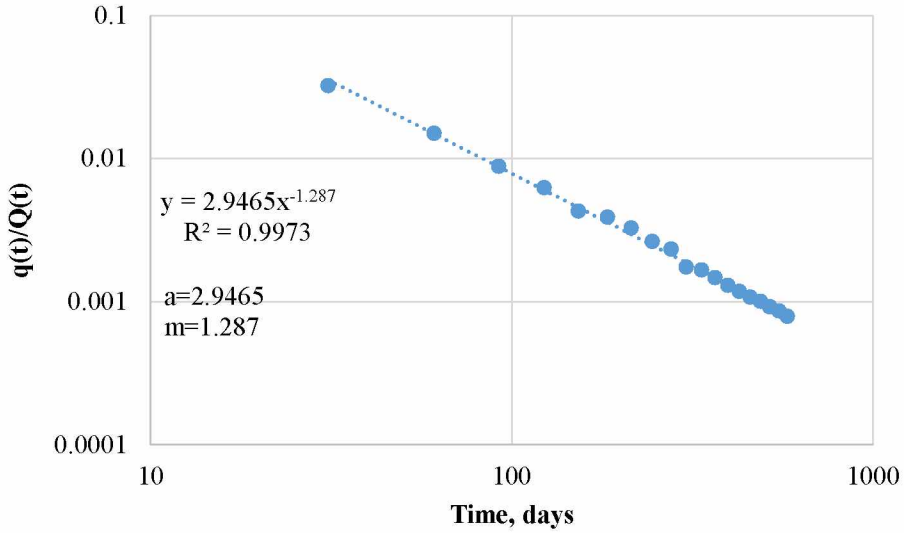

Figure 2.6: Example determination of *a* and *m* parameters for Duong's model

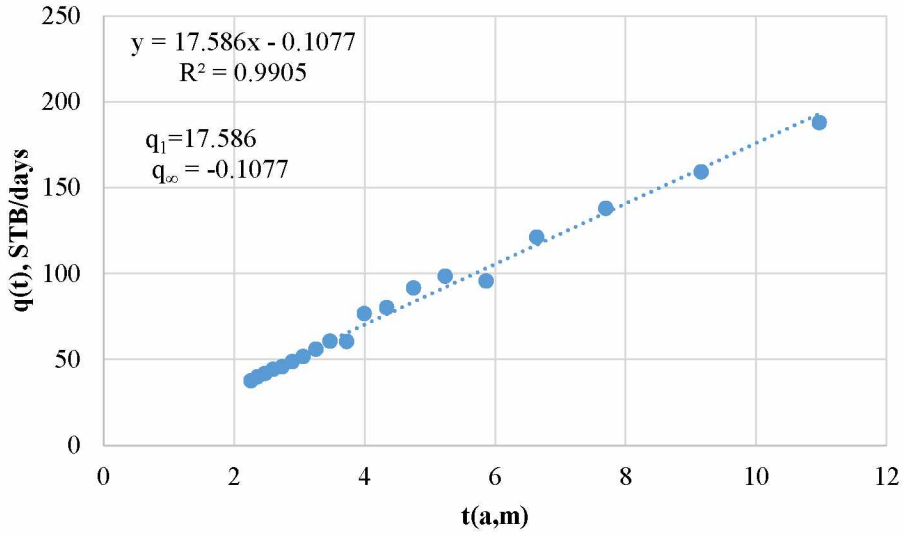

Figure 2.7: Example determination of q_1 and q_∞ parameters for Duong's model

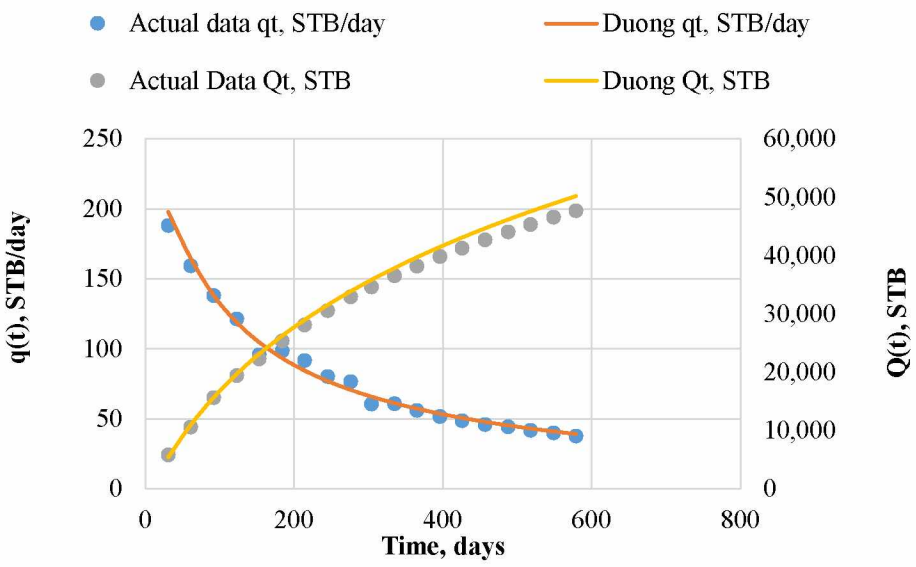

Figure 2.8: Example of Duong's model history match of Berry well (Karnes County)

2.6 Power law exponential

The power law exponential model was developed by Ilk and others in 2008 and applied to field examples by McNeil and others in 2009. It approximates shale gas wells' production rate decline with a power law decline. This model replaces the b and D_i values from Arps' model with the new parameters D_1, D_∞, and n', and its rate time takes the following form (equation (7)):

$$D = D_\infty + D_1 t^{-(1-n')} \tag{5}$$

$$q = \hat{q}_i \exp\left(-D_\infty t - \left(\frac{D_1}{n}\right) t^{n'}\right) \tag{6}$$

$$q = \hat{q}_i \exp\left(-D_\infty t - \hat{D}_i t^{n'}\right) \tag{7}$$

The major advantages of this model are: (1) the extra variables enable the model to account for both transient and boundary-dominated flow whenever necessary; and (2) the equation for production rate looks similar to Arps' exponential form, which gives the model a familiar feel.

It was observed that the power law model gives good estimates for reserves even with a short production history. The power law model was applied to 100 wells in the Eagle Ford Shale play. The least square regression between the PLE rate and the actual rate is minimized using Excel's multivariable solver tool. The time to reach abandonment was computed by equating production rate to 2 STB/day. The EUR can be estimated by integrating the rate with respect to time, as shown in equation (8):

$$Q(t) = \int_0^t \hat{q}_i \exp\left(-D_\infty t - \hat{D}_i t^{n'}\right) dt \tag{8}$$

The solution to this integral is not a trivial process. Alternatively, a good approximation for computing the EUR is accomplished numerically by summing up incremental production on a monthly basis until the abandonment rate of 2 STB/day is reached. We can also use the trapezoidal method to solve equation (8). If so, we have the following, equation 9:

$$Q(t) = \sum_{i=1}^{x} q(t)_i t_i \tag{9}$$

Figure 2.9 shows rate versus time series data for the Muenchow well in Karnes County along with both hyperbolic and power law fits. As seen in the figure, both models fit the production data very well; however, the hyperbolic model fits with a b value of 1.44, which, mathematically, leads to an unreliable estimate of remaining reserves. The power law fit overcomes this shortcoming, as it will terminate at a reasonable time to give more conservative results.

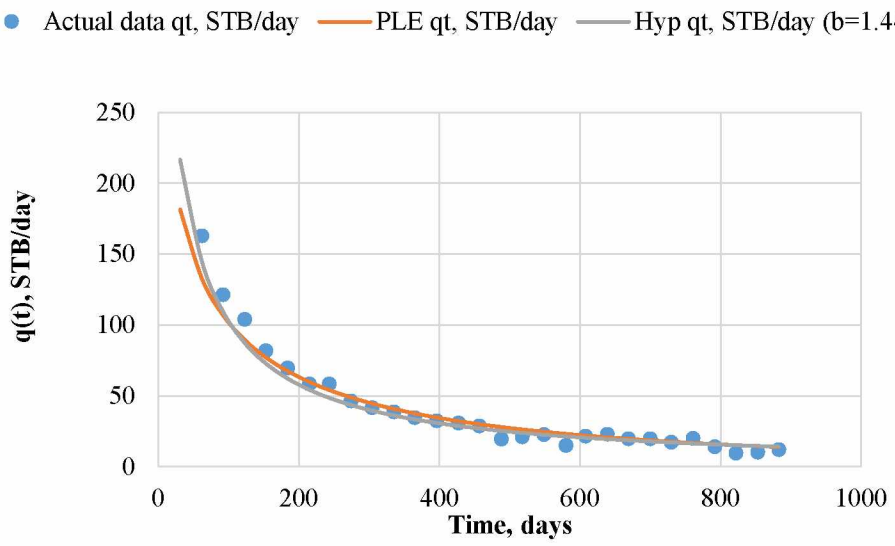

Figure 2.9: Hyperbolic and PLE fit for Muenchow well in Karnes County

2.7 Eagle Ford Shale – discussion of results

Based on the results from the diagnostic plot in Figure 2.3, the pie chart in Figure 2.10 shows that the majority of the wells (76%) are still in linear transient flow. According to this diagnosis, 24% of the wells have felt their boundary.

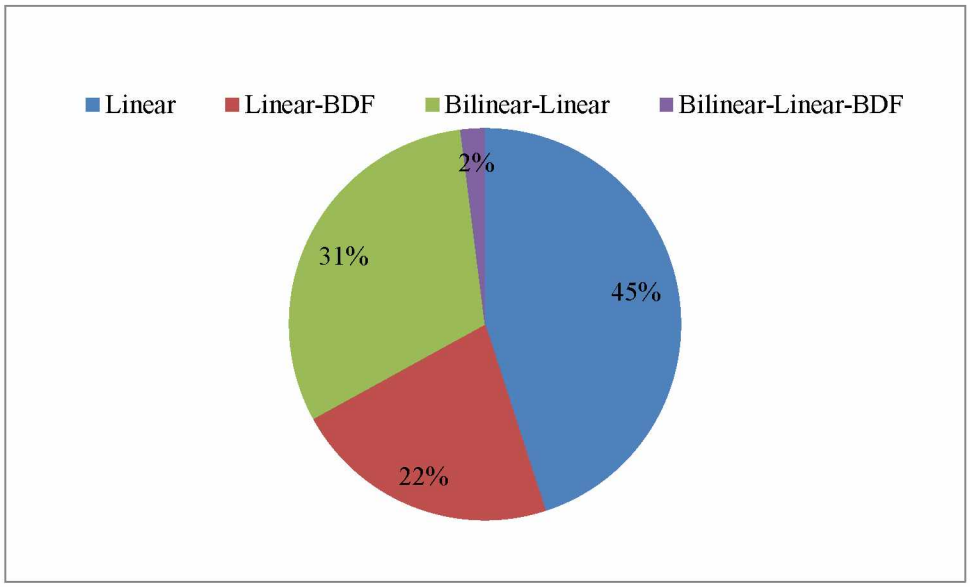

Figure 2.10: Percentage of flow regimes for 100 wells

The counties of the Eagle Ford Shale play have been categorized based on the type of flow regimes their wells follow. Accordingly, a detailed discussion and summary of the results of three counties are included in the following subsections: Karnes County, where there is a combination of both linear transient and boundary-dominated flow regimes; Burleson County, where all three wells analyzed have reached their boundary; and Zavala County, where all the wells are still flowing in a linear transient phase, though a few of them are preceded by bilinear flow. A brief discussion and summary is also included for the remaining five counties, which each fit in one of the categories just described and consistently follow similar trends.

2.7.1 Karnes County

Karnes County shows diverse results for flow regimes, with 29% of wells reaching boundary-dominated flow and 71% still in linear transient flow. In view of these results, the hyperbolic exponents are abnormal for 59% of the wells. Note that with the hyperbolic model, the time predicted to reach the abandonment rate depends heavily on flow regimes. A well that has reached its boundary-dominated flow frequently will have an exponent close to normal and, subsequently, will take less time to reach abandonment.

Figure 2.11 and Figure 2.12 show the results for EUR forecasts and abandonment time for 21 wells in Karnes County. The EUR forecasts using the LGA model are close to those of Arps' hyperbolic and harmonic models when the hyperbolic exponent is $b \leq 1$, implying that the LGA model can be relied upon in such cases. For cases where the hyperbolic exponent b is greater than unity, the LGA EUR forecasts a conservative value somewhere between the exponential and the harmonic forecast; thus, it constrains the recoverable reserves parameter K and provides more rational and logical forecasts.

Duong's model gave a slightly positive version of the LGA forecasts for all the wells with an abnormal hyperbolic exponent (Figure 2.11). However, Duong's model fitted only those wells with long enough production data with less noise. For cases with a short production history, the major disadvantage of Duong's model was extremely high or low reserve estimates. For wells with normal hyperbolic exponents, Duong's model gave reserve estimates close to the LGA results. The estimates for time remaining to reach abandonment (Figure 2.12) cannot be relied upon with this model for the simple reason that when the value of parameter $q\infty$ is positive and greater than 2

STB/day, the model gives unreasonably high results. For negative values of $q\infty$, the results for time remaining to reach abandonment are extremely low; this is because $q\infty$ is the rate at infinite time, which is obtained from the intercept of the diagnostic plot of rate versus time function, and therefore should not be restricted to any other value. Conversely, when the term $q\infty$ is completely eliminated, the results seem to match with those of the other models.

The PLE consistently forecasted the lowest reserves for all the wells in Karnes County. This model follows a similar trend as the LGA model. For cases where the hyperbolic exponent is normal, the PLE results are in good agreement with the hyperbolic model. When the hyperbolic exponent is abnormal, the PLE terminates production at reasonable values to give the most conservative EUR forecasts of all existing models. However, for Karnes County, the results for abandonment time using the PLE model fall between the exponential and LGA results.

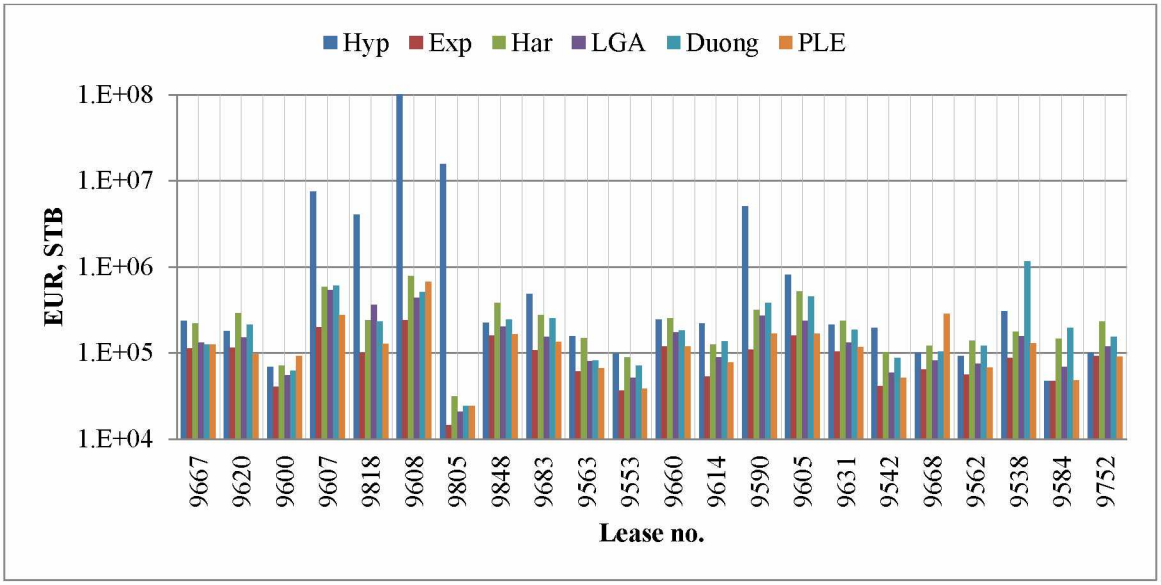

Figure 2.11: Karnes County EUR forecasts to abandonment rate of 2 STB/day

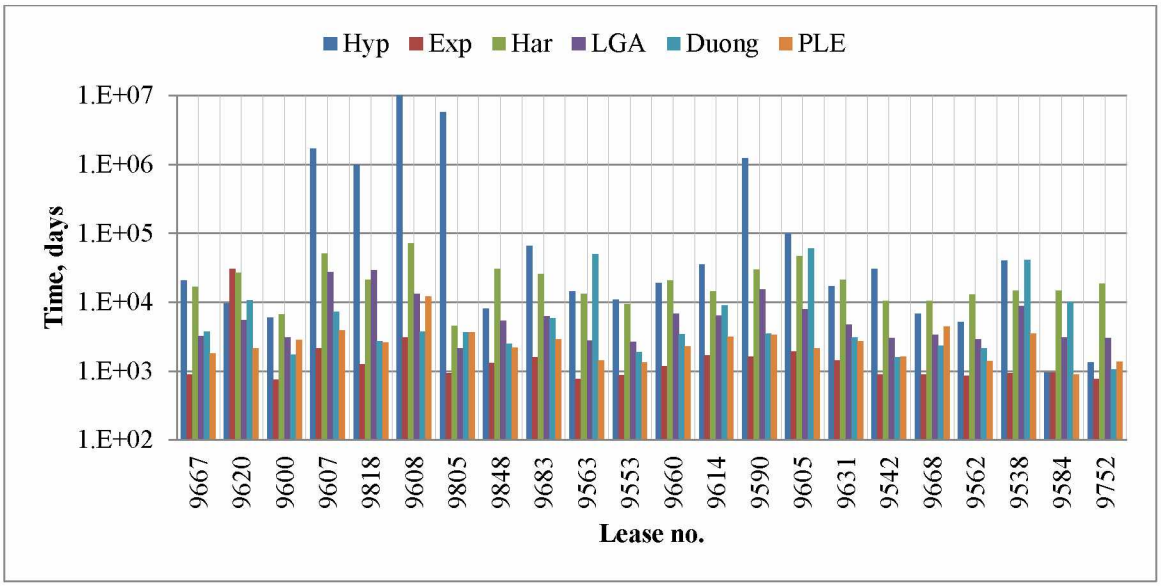

Figure 2.12: Karnes County time to reach abandonment rate of 2 STB/day

Table 2.1 summarizes the average EUR results for the 22 wells in Karnes County using all of the aforementioned models. For the hyperbolic model, only the wells having values of $b \leq 1.5$ are considered, as the values of $b > 1.5$ give extremely unreasonable estimates. The last row of Table 2.1 summarizes the percentage of wells following the respective decline model based on $R^2 \geq 0.95$ criteria for the respective history match; it also shows the standard deviations and the minimum, maximum, and median values for each of the models. From the table, a range of results is observed, from highly optimistic values with hyperbolic and harmonic models, to conservative forecasts with the LGA and PLE models, to mediocre forecasts with the Duong's model. The EUR estimates for Karnes County with the LGA and PLE models are comparable to each other. A higher percentage of wells give a good history match using these models. Duong's model predicts higher EUR estimates than the LGA and PLE models, but restricts the forecasts when compared with the hyperbolic model. It can be inferred from the results that the PLE gives the most conservative estimates for Karnes County.

Similarly, Table 2.2 summarizes the abandonment times to reach 2 STB/day for Karnes County for each of the models. From the table, a wide range of results is observed, from 63.8 years for the hyperbolic model, to 8.1 years for the PLE model.

Table 2.1: Average reserve estimates for Karnes County

Karnes	Hyp	Exp	Har	LGA	Duong	PLE
EUR(MSTB)	221.9	96.2	248.2	165.2	247.4	142.4
st. dev	184.3	55.6	180.6	131.6	251.2	135.9
min	47.1	14.4	31.4	20.9	24.3	24.3
max	809.7	238.0	777.7	533.6	1152.1	673.7
median	196.0	95.9	224.1	132.4	184.9	118.3
percentage	19.0	4.8	28.6	77.5	44.0	63.0

Table 2.2: Average producing life for Karnes County

Karnes	Hyp	Exp	Har	LGA	Duong	PLE
time (years)	63.8	7.2	62.0	20.9	29.1	8.1
st. dev	71.4	17.4	44.6	20.9	46.3	6.3
min	2.6	2.1	12.6	5.9	2.9	2.5
max	273.9	84.6	198.9	80.3	166.7	33.9
median	40.3	3.0	48.8	14.0	9.9	6.7
percentage	19.0	4.8	28.6	77.5	44.0	63.0

2.7.2 Burleson County

Analysis of three wells from Burleson County showed that all have reached boundary-dominated flow. Note that a good history match with Arps' normal hyperbolic exponent is obtained for the wells that have felt their boundary. Accordingly, two of the wells have a normal exponent.

Figure 2.13 shows the EUR forecasts for three wells from Burleson County to the abandonment rate of 2 STB/day. The EUR estimates using the hyperbolic and harmonic models depend greatly on the exponent value. For abnormal exponents, the hyperbolic model gives optimistic results. In fact, for *b* values greater than 2, EUR estimates are irrationally high. The harmonic model tends to curve down these estimates.

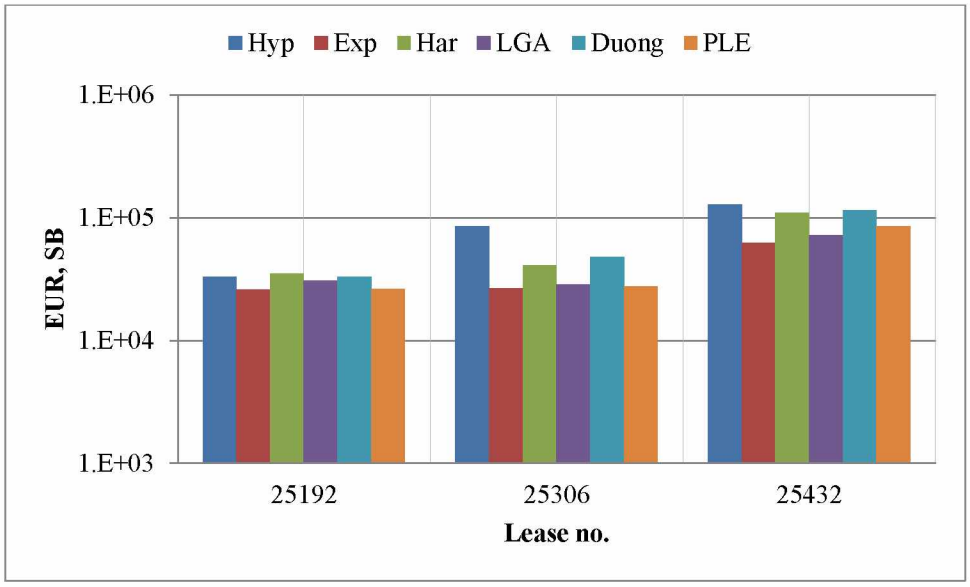

Figure 2.13: Burleson County EUR forecasts to 2 STB/day

The Giesenschlag W.H. and the Giesenschlag-Groce wells history matched well with hyperbolic and harmonic decline and exponents of 0.96 and 1.06, respectively. Consequently, these two wells gave agreeable results with the LGA model, indicating its reliability with normal exponent values. On the other hand, the A.B. Childers well had a hyperbolic exponent of 1.66, and LGA EUR forecasts were more conservative, with an EUR forecast value between harmonic and exponential results.

The Giesenschlag W.H. and the Giesenschlag-Groce wells history matched well with Duong's model, again giving reserve estimates comparable with those of Arps' and LGA models. For the A.B. Childers well, Duong's model gave reserve estimates higher than those of the LGA model, but slightly lower than Arps' harmonic results.

The PLE model followed a similar trend as the LGA model, thus giving conservative results and indicating reliability of the PLE and LGA models for more realistic and reasonable forecasts. Figure 2.14 shows the time to reach abandonment rate of 2 STB/day for the three wells in Burleson County. Note that that abandonment time follows a similar trend as EUR.

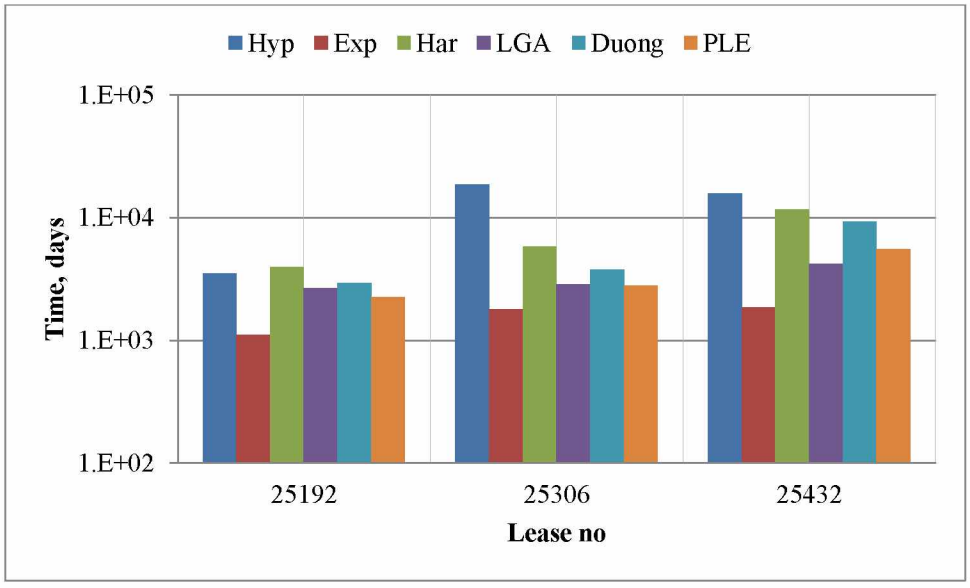

Figure 2.14: Burleson County time to reach abandonment rate of 2 STB/day

Table 2.3 summarizes the average EUR results for the three wells in Burleson County from all models and shows the percentage of wells following the respective declines based on $R^2 \geq 0.95$ criteria for the respective history matches.

Table 2.3 also shows the standard deviations and minimum, maximum, and median values for each of the models. From the table, a range of results is observed, from the highly optimistic values of the hyperbolic model, to conservative forecasts with the LGA and PLE models, to mediocre forecasts with the Duong's model. The EUR estimates for Burleson County with the LGA and PLE models are comparable to each other, and a higher percentage of wells give a good history match using these two models. For the hyperbolic model, only the wells having values of $b \leq 1.5$ are considered, as the values of $b > 1.5$ give extremely unreasonable estimates. Duong's model predicts higher EUR estimates than the LGA and PLE models, but restricts the forecasts as compared with the hyperbolic model.

Table 2.4 summarizes the average abandonment times to 2 STB/day for Burleson County for each of the models. From the table, a wide range of results is observed, from 35.2 years for the hyperbolic model, to as low as 9 years for the LGA model.

Table 2.3: Average reserve estimates for Burleson County

Burleson	**Hyp**	**Exp**	**Har**	**LGA**	**Duong**	**PLE**
EUR(MSTB)	82.4	38.2	62.1	43.8	65.4	46.4
st. dev	47.6	20.8	41.7	24.6	43.8	33.5
min	33.2	25.9	35.1	28.7	33.1	26.4
max	128.4	62.2	110.2	72.2	115.3	85.1
median	85.7	26.6	41.2	30.6	47.9	27.7
percentage	33.34	0	66.7	66.7	33.34	33.34

Table 2.4: Average producing life for Burleson County

Burleson	Hyp	Exp	Har	LGA	Duong	PLE
time (years)	35.2	4.4	19.9	9.0	14.8	9.8
st. dev	22.4	1.1	11.3	2.4	9.6	4.9
min	9.7	3.1	11.1	7.4	8.2	6.3
max	51.7	5.1	32.7	11.7	25.9	15.4
median	44.1	5.0	16.1	7.9	10.4	7.8
percentage	33.34	0	66.7	66.7	33.34	33.34

2.7.3 Zavala County

All 15 wells in Zavala County are in the linear transient flow regime. In cases where a well is in linear transient flow, the production history matches well with Arps' hyperbolic exponent values, frequently lying between 2 and 4.

Figure 2.15 and Figure 2.16 show forecasts and abandonment for fifteen wells in Zavala County. Again, the LGA model fits all the wells in a good manner and predicts reasonable reserves for EUR and time to reach abandonment rate of 2 STB/day as compared with abnormal hyperbolic exponent wells.

Although the history match for Duong's model is not good, the reserve estimates for most wells in Zavala County are comparable to those of the LGA model and Arps' model when the hyperbolic exponent is normal. Similar to wells in Karnes County, when q_∞ is non-zero, the results for time to reach abandonment are extremely high or low, respectively.

The PLE model fits most of the wells' past production data; it follows a similar trend as LGA and has the lowest forecasts of all the models.

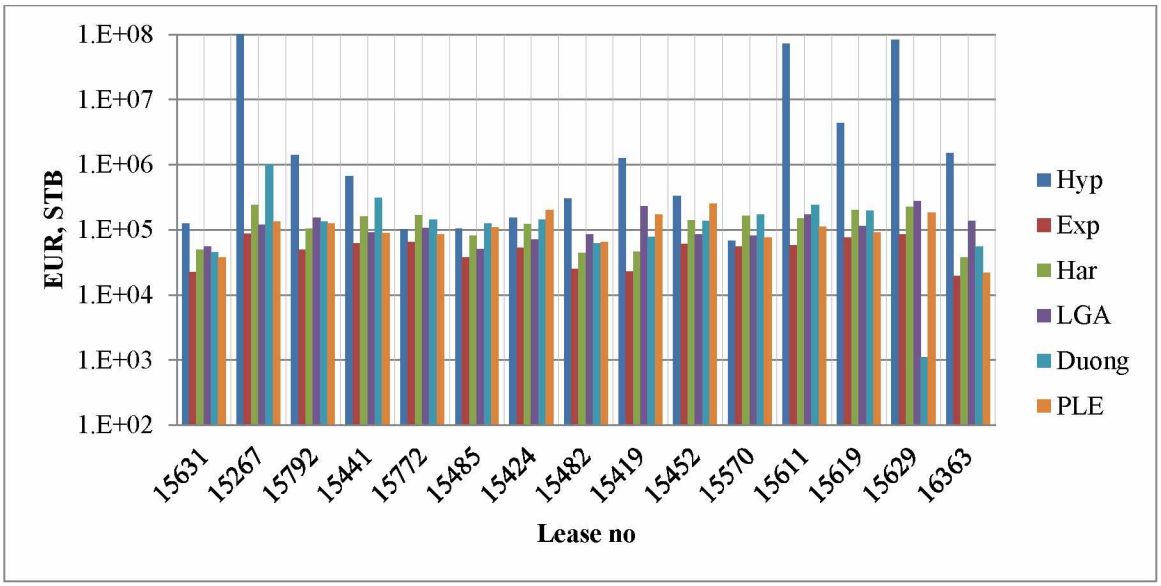

Figure 2.15: Zavala County EUR forecasts to abandonment rate of 2 STB/day

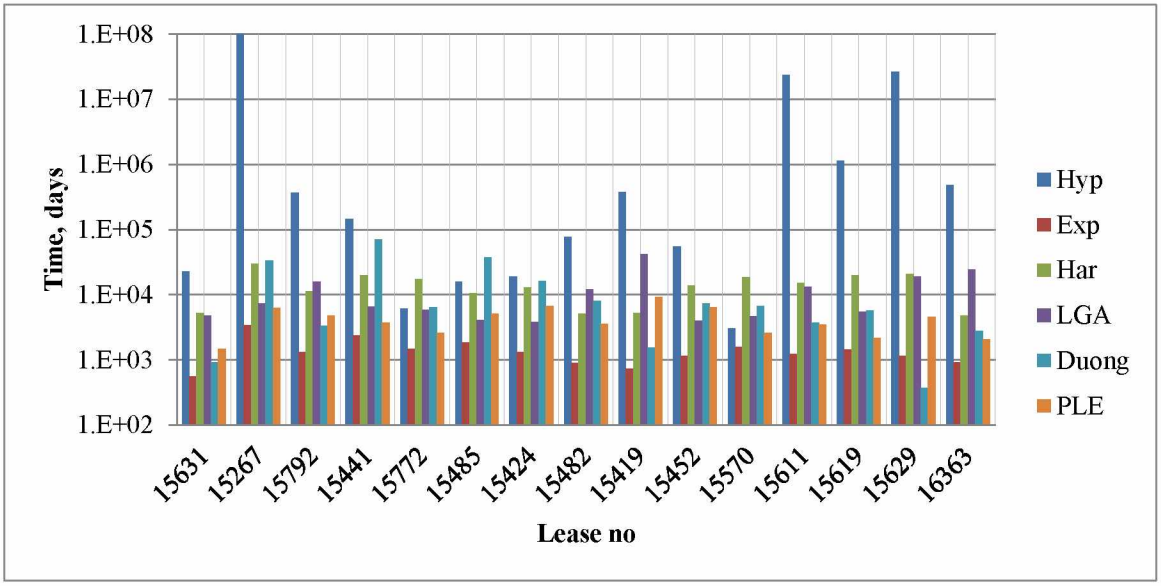

Figure 2.16: Zavala County time to reach abandonment rate of 2 STB/day

Table 2.5 summarizes the average EUR results for the fifteen wells in Zavala County using all the aforementioned models. For the hyperbolic model, only the wells having values of $b \leq 1.5$ are considered, as the values of $b > 1.5$ give extremely unreasonable estimates. The last row in the table summarizes the percentage of wells following the respective declines based on the $R^2 \geq 0.95$ criteria for the respective history matches.

Table 2.5 also shows the standard deviations and the minimum, maximum, and median values for each of the models. From the table, a range of results is observed, from the highly optimistic values of the hyperbolic and harmonic models, to conservative forecasts with the LGA and PLE models. The EUR estimates for Zavala County with the LGA and PLE models are comparable to each other and a higher percentage of wells give a good history match using these models. The Duong's model predicts higher EUR estimates than those of the LGA and PLE models, but restricts the forecasts as compared with the hyperbolic model. Thus, it can be inferred from the results that the PLE gives the most conservative estimates for Zavala County. Therefore, even when the flow regimes of the wells are transient, the trend followed by various techniques does not differ much.

Figure 2.6 summarizes the abandonment times to 2 STB/day for Zavala County for each of the models. From the table, a wide range of results is observed, from 56.4 years for the hyperbolic model to as low as 12 years for the PLE model.

Table 2.5: Average reserve estimates for Zavala County

Zavala	Hyp	Exp	Har	LGA	Duong	PLE
EUR(MSTB)	147.6	51.8	129.2	122.1	188.9	116.4
st. dev	94.8	22.2	66.8	64.2	236.3	62.6
min	68.6	19.5	37.8	50.6	1.1	21.7
max	332.6	86.8	241.3	278.9	993.2	252.2
median	114.9	54.3	140.6	106.4	135.8	110.2
percentage	14.3	0.0	0.0	91.0	59.6	80.0

Table 2.6: Average remaining producing life for Zavala County

Zavala	Hyp	Exp	Har	LGA	Duong	PLE
time (years)	56.4	4.0	38.9	32.1	37.9	12.0
st. dev	51.8	2.0	20.1	29.1	53.8	5.9
min	8.5	1.5	13.3	10.6	1.0	4.1
max	153.1	9.5	82.9	115.6	196.7	25.6
median	48.1	3.7	38.2	18.2	18.0	10.3
percentage	14.3	0.0	0.0	91.0	59.6	80.0

2.7.4 Remaining counties

Figure 2.7 through Figure 2.11 report the average EUR and abandonment time results for Gonzales, La Salle, Live Oak, Dimmit, and De Witt counties. The first row in the tables shows the number of wells analyzed in each county. The last row in the tables reports the percentage of wells that follow the respective models. For the hyperbolic model, only the wells having b values ≤ 1.5 are considered. The key point to note here is that the LGA and the PLE consistently remain the most successful in matching the past performance of all the counties. A second key point is that the overall results from these two models are comparatively closer to each other, implying more dependability. Of the two models, the PLE gives lower estimates for reserves and abandonment time. Duong's model has the next best success in terms of history match; its overall results for reserve estimates are relatively higher than LGA results, but they still seem reasonable compared with Arps' hyperbolic results. Therefore, Duong's model can be considered an optimistic way of predicting well performance.

Table 2.7: Average reserve estimates and producing life for Gonzales County

	Hyp	Exp	Har	LGA	Duong	PLE
EUR(MSTB)	157.3	65.3	139.8	92.7	99.1	80.7
st.dev	117.8	26.1	93.7	32.5	75.3	40.4
time (years)	41.2	4.1	35.1	13.5	19.5	11.7
st.dev	31.7	2.3	31.2	7.3	13.7	7.4
percentage	33.3	6.7	13.3	80.0	46.7	86.7

Table 2.8: Average reserve estimates and producing life for La Salle County

	Hyp	Exp	Har	LGA	Duong	PLE
EUR(MSTB)	230.5	63.6	180.8	120.3	201.7	98.3
st.dev	207.5	54.7	142.9	79.4	175.5	53.1
Time (years)	55.6	3.0	46.5	22.2	25.7	15.7
st.dev	42.3	1.0	25.1	9.6	19.5	8.5
percentage	26.3	0.0	15.8	63.9	33.8	40.2

Table 2.9: Average reserve estimates and producing life for Live Oak County

	Hyp	Exp	Har	LGA	Duong	PLE
EUR(MSTB)	777.3	156.0	418.6	331.6	566.2	302.6
st.dev	699.6	134.1	330.7	218.8	492.6	163.4
Time (years)	98.9	3.9	96.1	40.4	52.1	32.7
st.dev	75.2	1.2	51.9	17.4	39.6	17.7
percentage	20.0	0.0	20.0	80.0	60.0	80.0

Table 2.10: Average reserve estimates and producing life for Dimmit County

	Hyp	Exp	Har	LGA	Duong	PLE
EUR(MSTB)	131.9	47.9	114.4	69.2	97.8	67.1
st.dev	105.5	41.2	81.3	60.9	39.1	15.4
Time (years)	46.6	3.6	35.4	12.7	17.6	10.5
st.dev	35.4	1.2	19.1	5.5	13.4	5.7
percentage	25.0	0.0	25.0	100.0	75.0	75.0

Table 2.11: Average reserve estimates and producing life for De Witt County

	Hyp	Exp	Har	LGA	Duong	PLE
EUR(MSTB)	1901.5	396.2	1488.3	606.7	2325.2	534.6
st.dev	1521.2	340.7	1056.7	533.9	930.1	122.9
Time (years)	72.2	6.9	60.3	38.0	80.3	30.0
st.dev	54.9	2.2	32.6	16.4	61.0	16.2
percentage	44.4	0.0	22.2	88.9	55.6	77.8

2.8 Summary of deterministic DCA models

Analysis of 100 wells using different decline models highlights some of the pitfalls associated with using DCA models developed for conventional reservoirs in shale wells. For 60 of the wells the hyperbolic b values were higher than one. Arps' hyperbolic equation consistently provided high estimates and may be said to be the optimistic approach for generating future production predictions due to the unusually high Arps' decline b exponent. As stated elsewhere in the technical literature, forecasting transient production using Arps' hyperbolic equation with b>1 can lead to a severe overestimation of EUR, and for that matter, remaining reserves.

Overall, the LGA model fits 81% of the wells' past production rates and cumulative production. The lack of a good history match with the remaining wells may be due to paucity of production history data. The LGA model gives finite EUR estimates when compared to Arps' models.

Duong's model fits the production rates and cumulative production data for about 51% of the wells. Duong's model performed well when the production history was at least 20-24 months with minimal noise. However, for some cases, even when the data was smoothed, Duong's model did not match the production history well. It also resulted occasionally in extremely high reserve estimates, like Arps' hyperbolic model, or extremely low reserve estimates, like Arps' exponential model, with no clear cause.

As PLE comes from the exponential family of curves, it is similar to Arps' exponential model. For other cases, the PLE consistently gave the lowest forecasts of all the models. Therefore, it is the most conservative method for production forecasting and reserve estimation. Based on $R^2 \geq 0.95$, PLE fits 67% of the wells' past production rates.

The comparison in terms of percentage fitted by each model and remaining reserve/remaining life for each model is shown in Figure 2.17. Based on Figure 2.18, LGA, which also reports conservative results, remains the most successful model to match the wells' past production performance. Thus it can be inferred that LGA, PLE, and Duong's models do overcome the limitations of Arps' model to a certain extent when applied to shale reservoirs. However, there is still scope for a better model in terms of consistency in fitting the wells' past production.

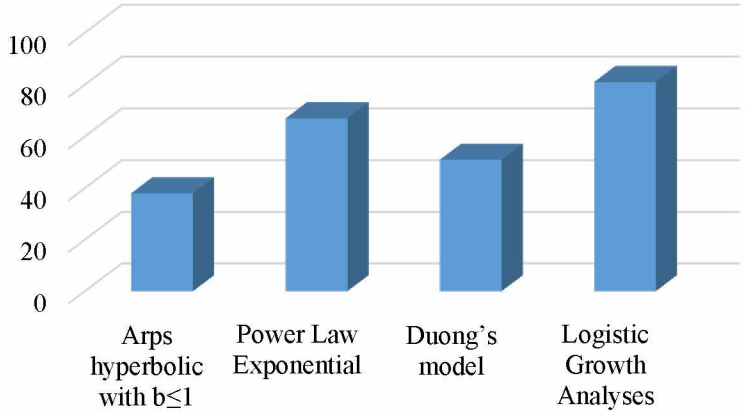

Figure 2.17: Bar chart showing percent fitted based on a regression coefficient of 95% by investigated models

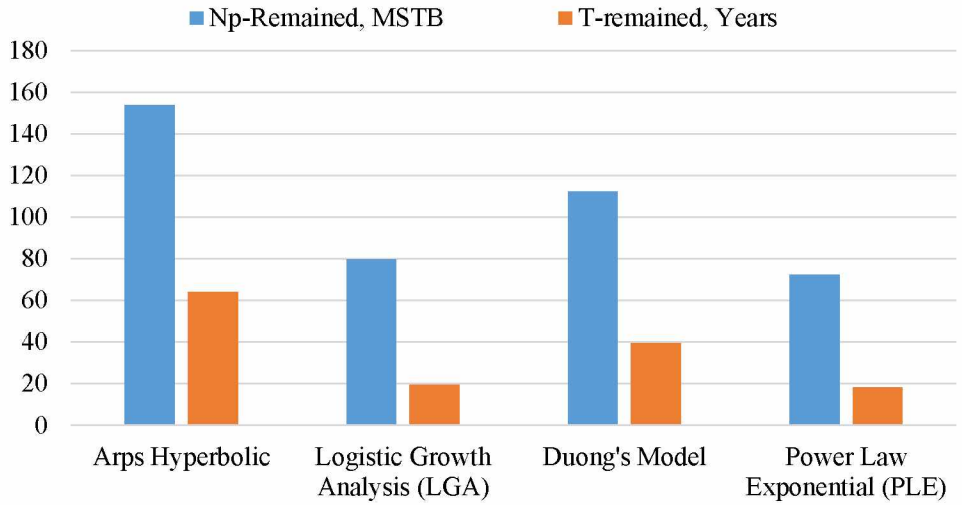

Figure 2.18: Bar chart comparing performance of investigated models

Chapter 3. Influence of Residual Function Form on the Performance of Deterministic Models

3.1 Introduction

Numerous efforts have been made to overcome the shortcomings associated with using Arps' models for production data analysis in unconventional reservoirs. The three models reviewed in Chapter 2 overcome the limitations of Arps' models to varying degrees, with the LGA and PLE models making the most conservative predictions and Duong's model falling in between LGA and PLE. Arps' hyperbolic and the LGA equation provided the most optimistic/pessimistic reserve estimates, respectively. However, Arps' model is still widely used for the evaluation of EUR of shale oil/gas wells, probably because of its simplicity. Therefore, to improve the applicability of Arps' model, this thesis investigates how the choice of residual function affects the estimate of model parameters and consequent remaining well life and reserves.

3.2 Using different residual functions to improve forecasting

In the above study, monthly oil production data is deterministically fitted for each well by constraining the parameters using least residual squares. The residual used for that work is the least square error computed using the fit from the above models and actual rate/cumulative data. Hereafter, this is called the base error function. When this error form is used, earlier data points are more heavily weighted. This affects the resulting model parameters and subsequent forecasts.

To address this problem, two and four different residual functions were defined and used for cumulative-time and rate-time forms, respectively (Table 3.1). The objective of the proposed residuals is to weigh the most recent production data more heavily. This will ensure that the fitted parameters will reflect the current flow regime in the drainage area of the wells. LGA and Arps' models were applied to the data using the new residual functions. This process was integrated in Excel-VBA spreadsheet software.

Table 3.1: Error functions used for analysis

Residual Function Name	Residual Function Equation
Base Error function	$\sum(q_{actual} - q_{calculated})^2$
Normalized rate	$\sum\left(1 - \frac{q_{calculated}}{q_{actual}}\right)^2$
Inverse Normalized rate	$\sum\left(\frac{1}{q_{actual}} - \frac{1}{q_{calculated}}\right)^2$
Cumulative	$\sum(Q_{actual} - Q_{calculated})^2$
Normalized cumulative	$\sum\left(1 - \frac{Q_{calculated}}{Q_{actual}}\right)^2$
Logarithmic rate	$\sum Abs\left[\ln\left(\frac{q_{actual}}{q_{calculated}}\right)\right]$

3.3 Example case study

Figure 3.1 shows the various fits of production data from Oliver B well in the De Witt County and the different residual functions. Table 3.2 summarizes the performance of Arps' and LGA models using different error functions with the same data. The base case residual function fits the trend hyperbolically with a b value of 0.76, whereas the normalized rates, inverse normalized rates, and logarithmic residuals fit with b values of 0.41, 0.43, and 0.25, respectively. The cumulative residual function follows harmonic decline with a b value of 1 and normalized cumulative residual fits with a b value of 0.91. Because of the reduction in b-values for both the normalized rates and

logarithmic residuals, the predicted remaining life and remaining reserves drop substantially. This results in conservative forecasts comparable with LGA model results.

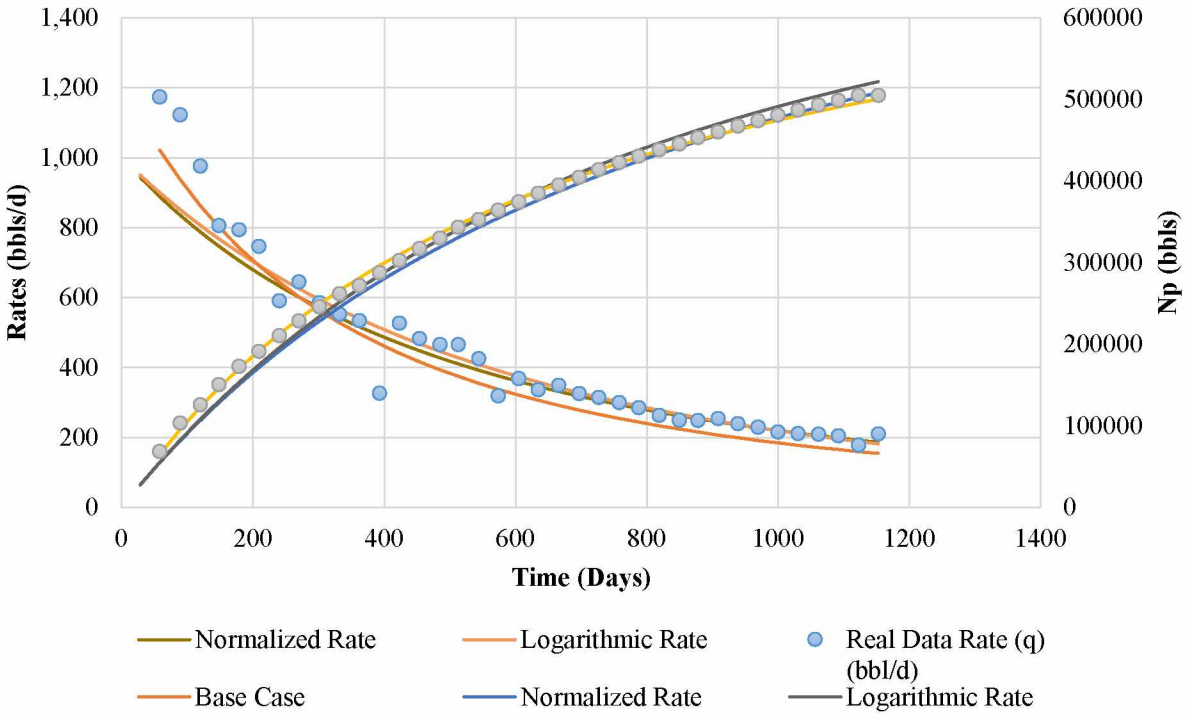

Figure 3.1: Influence of error function showing different fits for different error functions for Oliver B well

Figure 3.2 shows the various fits using data from Haug-Kieschnick Unit 33 in La Salle County and the different residual functions. Table 3.3 summarizes the performance of Arps' and LGA models using different error functions with the same data. The base case fits the trend hyperbolically with a b value of 1.49, whereas the normalized rates, inverse normalized rates, and logarithmic residuals fit with b values of 0.67, 0.29, and 0.66, respectively. Again in this case, using these different residual functions leads to lower b value estimates. This also results in conservative estimates. The cumulative residual error function follows hyperbolic decline with a b value of 1.36 and the normalized cumulative residual fits with a b value 1.84. (Note: since $b > 1$ gives unreasonable forecasts, the b value is restricted to 1 for the base case for illustration purposes).

Table 3.2: Results summary for proposed residuals applied to Oliver B well

Model	T-remained, days	Np-Remained, STB	Error Function	Fitting q or Q vs. time	b value
Hyperbolic	47127	659763	Base Case	q	0.76
Hyperbolic	12317	278718	Normalized Rate	q	0.41
Hyperbolic	13396	296967	Inverse Normalized Rate	q	0.43
Harmonic	132227	1234697	Cumulative	Q	1.00
Hyperbolic	85402	902057	Normalized Cumulative	Q	0.91
Hyperbolic	6910	210552	Logarithmic Rate	q	0.25
LGA	21350	388802	Base Case	Q	
LGA	16778	299729	Normalized	Q	

3.4 Residual function analysis: statistical analysis of parameters

The box and whisker plots in Figure 3.3-3.5 summarize the center, spread, and overall range of Arps' hyperbolic parameters b, D_i, and q_i after matching the model to 100 wells in the Eagle Ford Shale. Each of the four parts of the box plots represents 25% of the data set. The D_i boxplots for different error functions are typically skewed towards the bottom, implying that they usually follow log-normal distributions. The range of data values for normalized rates and logarithmic residuals is narrow compared to the spread of other cases. Unlike D_i values, the b boxplots are typically normally distributed and not skewed. Considering the hyperbolic decline for the base and cumulative cases, the majority of the values fall above the cutoff value of 1 with a mean of 1.2 and standard deviation of 0.7. However, the normalized rates and logarithmic residuals limit the b-values to varying degrees.

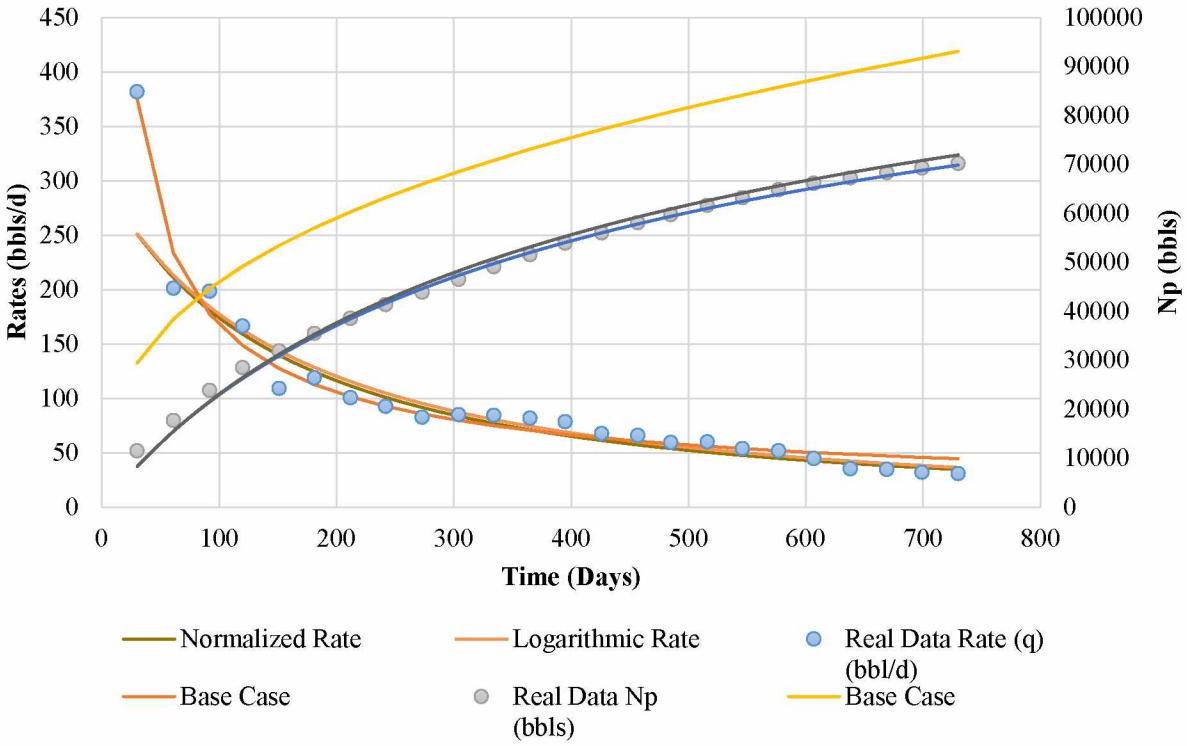

Figure 3.2: Influence of error function on parameter b for Haug Kieschnick Unit 33 well

This observation is strengthened in Figure 3.6, which shows the cumulative distribution functions (CDF) of the b values. The base case CDF shows that approximately 40% of the b values obtained are below 1. The normalized and logarithmic CDF shows that approximately 60% and 75% of the b values obtained using these residuals are below 1, respectively. It is interesting to note that almost 90% of the b values obtained fall below 1.5 with the normalized-rate and logarithmic-rate error functions.

Table 3.3: Results Summary for proposed residuals applied to Haug Kieschnick Unit 33 well

Model	T-remained, days	Np-Remained, STB	Error Function	Fitting q or Q vs time	b value
Harmonic	12487	87236	Base Case	q	1.00
Hyperbolic	5376	45767	Normalized Rate	q	0.67
Hyperbolic	1866	29434	Inverse Normalized Rate	q	0.29
Harmonic	13417	82538	Cumulative	Q	1.00
Harmonic	11500	66720	Normalized Cumulative	Q	1.00
Hyperbolic	5554	50389	Logarithmic Rate	q	0.66
LGA	5880	46613	Base Case	Q	
LGA	6000	44937	Normalized	Q	

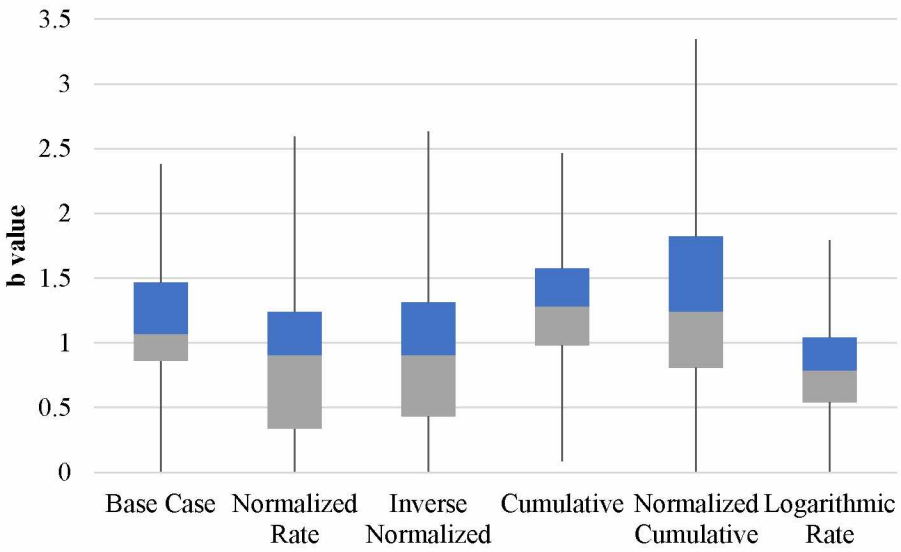

Figure 3.3: Box and whisker plot showing spread of b values for proposed residual functions

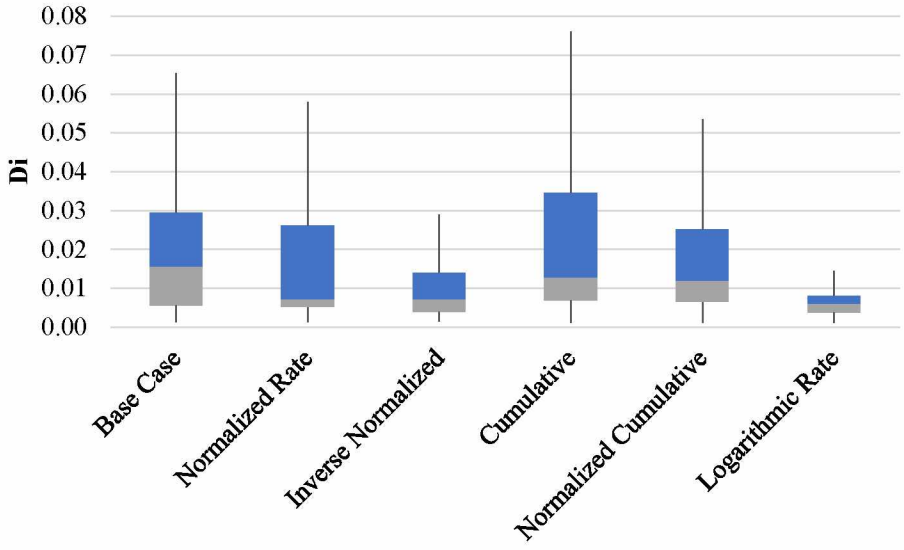

Figure 3.4: Box and whisker plot showing spread of D_i values for proposed residual functions

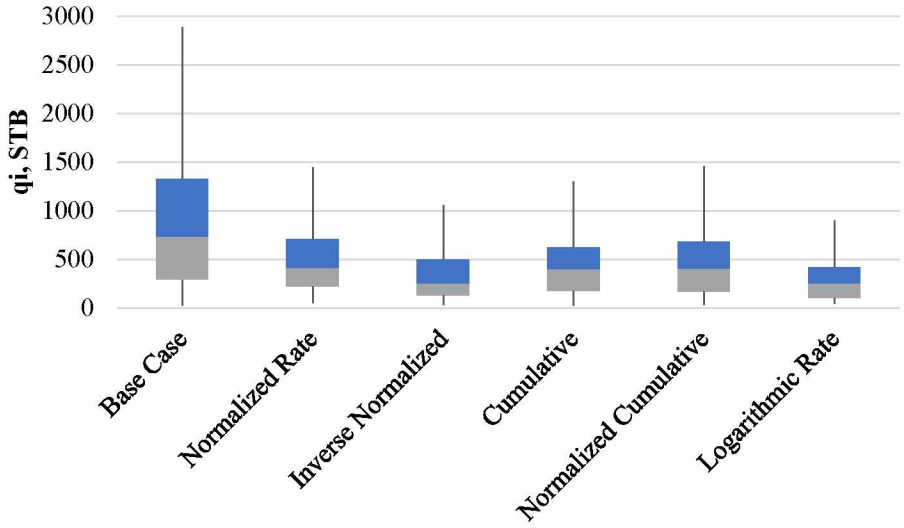

Figure 3.5: Box and whisker plot showing spread of q_i values for proposed residual functions

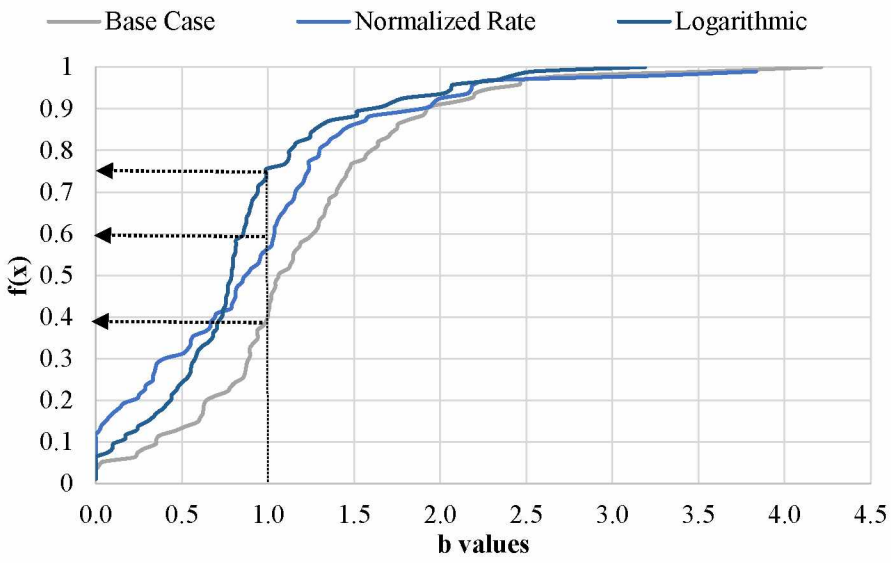

Figure 3.6: Cumulative distribution function for parameter b for proposed residual functions

3.5 Influence of residual function on remaining reserve and remaining life

The statistical analysis of remaining reserves and remaining life to an abandonment rate of 2 bbls/day was done on one hundred oil wells from the Eagle Ford Shale. Figure 3.7 and Figure 3.8 show that using the normalized and logarithmic rate-time residual forms increased the tendency of Arps' model to have bounded estimates of reserves. Figure 3.9 through 3.12 show the distributions of remaining reserves obtained from Arps' model using the base case residual function, normalized residual function, logarithmic residuals, and LGA models. The y-axis is the frequency count for the 100 wells analyzed. All four distributions are log-normally distributed as the high productivity wells do not occur frequently. Arps' base case forecasts a minimum of 50 MSTB and maximum of 900 MSTB for remaining reserves. Arps' normalized and Arps' logarithmic residuals forecast ranges of 15-500 MSTB and 50-500 MSTB, respectively, while the LGA range is 50-450 MSTB for the remaining reserves. This clearly shows that even though the b values are less than or equal to 1 for the base case, Arps' model will consistently provide optimistic results. On the other hand, the newly proposed residuals provide more realistic results, similar to those of LGA.

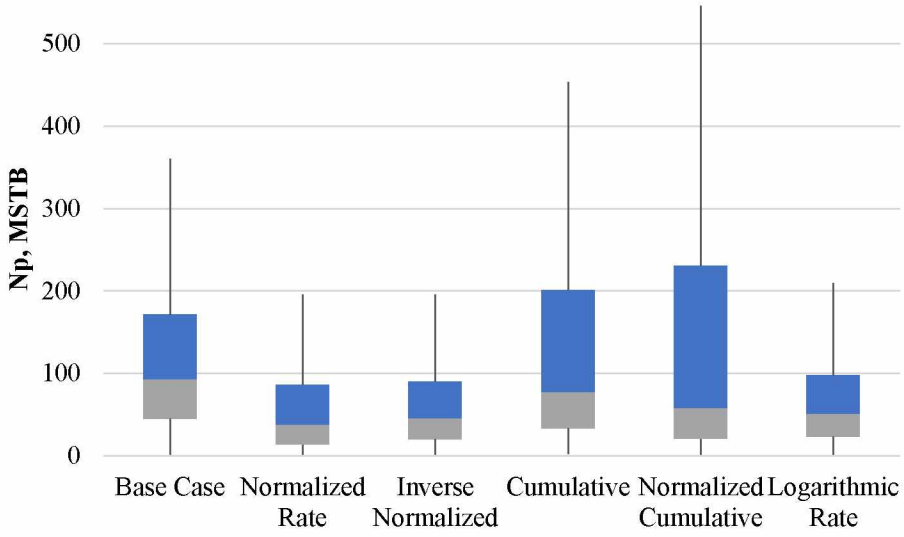

Figure 3.7: Box and whisker plot showing spread of remaining reserves for proposed residual functions

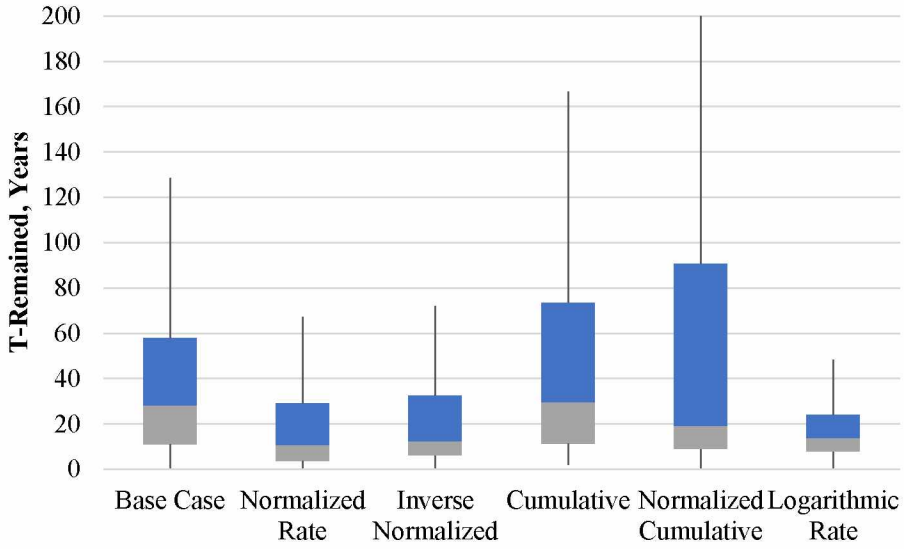

Figure 3.8: Box and whisker plot showing spread of remaining time for proposed residual functions

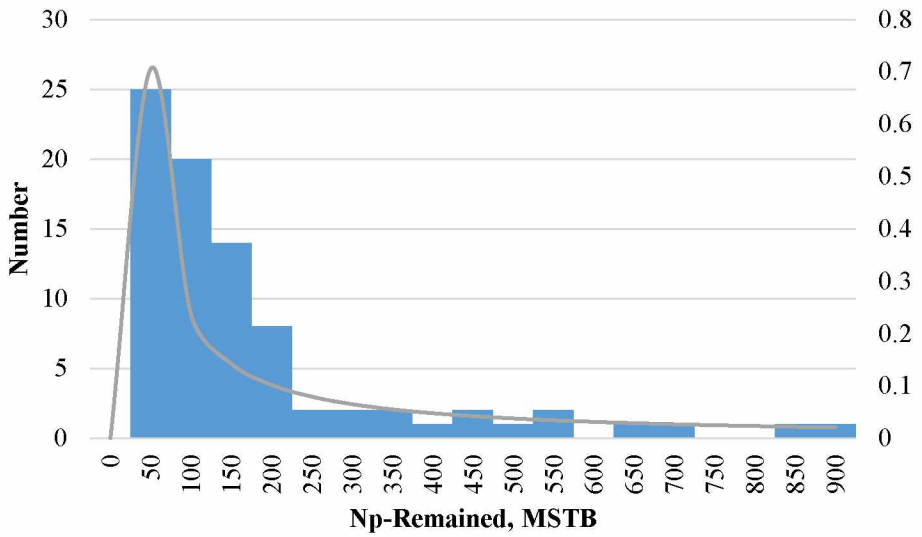

Figure 3.9: Distribution of remaining reserves with base case in Eagle Ford Shale

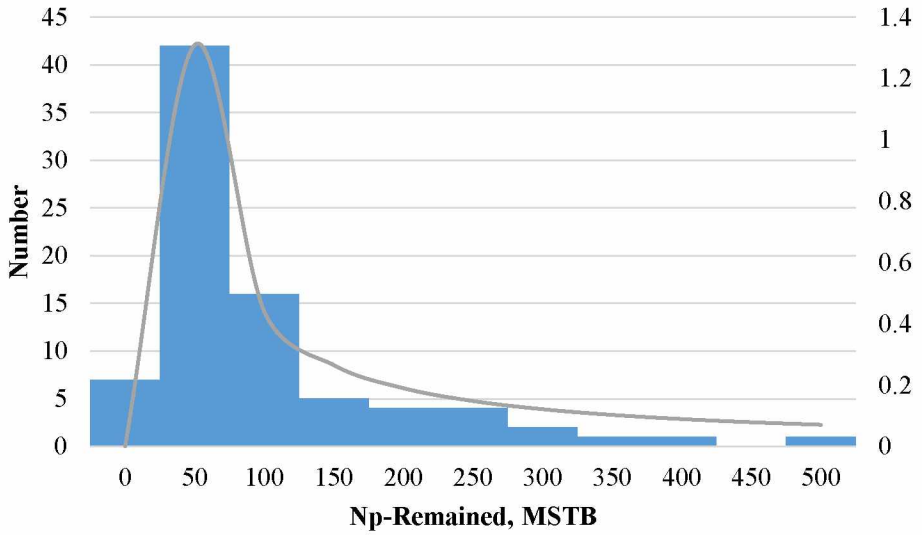

Figure 3.10: Distribution of remaining reserves with normalized residual

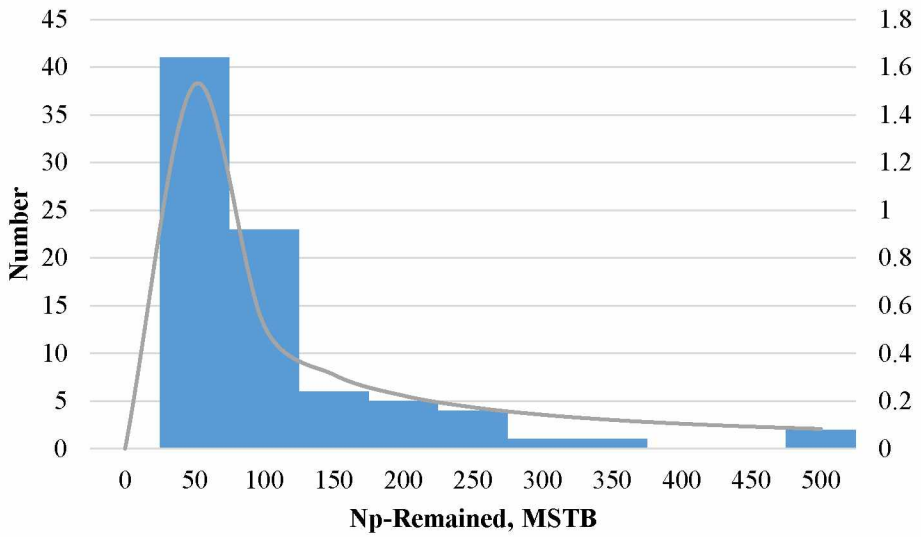

Figure 3.11: Distribution of remaining reserves with logarithmic residual

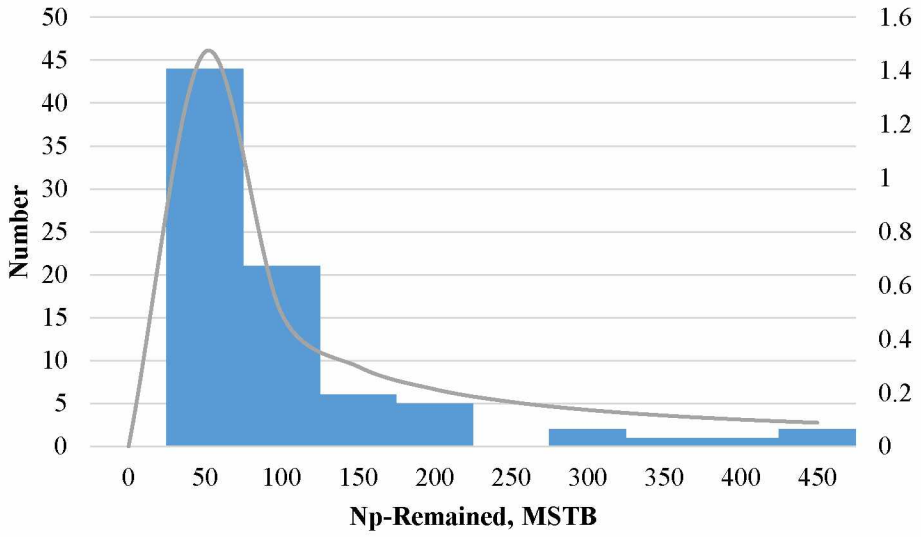

Figure 3.12: Distribution of remaining reserves with LGA

Chapter 4. Approximate Bayesian Computation for Probabilistic Decline Curve Analysis

4.1 Introduction to Bayes theorem

The proposed methodology is based on Bayes' theorem, equation 1:

$$\pi(\theta_j \mid y) = \frac{f(y \mid \theta_j) * \pi(\theta_j)}{\int f(y \mid \theta) * \pi(\theta) * d\theta} \tag{1}$$

where θ_j represents the DCA parameters, y represents the production data, $\pi(\theta_j)$ represents prior distribution, $f(y \mid \theta_j)$ represents likelihood function and $\pi(\theta_j \mid y)$ represents posterior distribution.

To apply Bayesian inference to the deterministic DCA models, the parameters are linked to Bayes' theorem by assuming the prior distribution is the distribution of DCA parameters before any production data have been observed. This can be a uniform distribution based on practical ranges of the parameters. The likelihood function is the conditional probability of the available production history given the DCA parameters. The posterior distribution is the distribution of the DCA parameters after all the available production history has been taken into account. In a Bayesian model, the goal is to compute the posterior distribution when some amount of data has been observed (Kruschke, 2011).

4.2 Probabilistic decline curve analysis

The probabilistic DCA methods published in the literature include the bootstrap method developed by Jochen and Spivey (1996); the modified bootstrap method (MBM) developed by Cheng and others (2010); and the Markov Chain Monte Carlo method (MCMC) developed by Gong and others (2014). The bootstrap method is a statistical method where the given data set is directly sampled in order to evaluate the probability of production forecasts. Therefore, no knowledge of priors is needed. We can use the bootstrap method to acquire statistical knowledge of many real problems such as noise in production data.

The bootstrap method starts with generating a large number of synthetic data sets from the original data set itself. Each synthetic set is of the same number of data points as the original data set. In

conventional bootstrap method, random samples are generated from the production data while replacing the drawn samples in the original data set. Thereafter, each of the synthetic data set is described using Arps' hyperbolic model and nonlinear regression in order to obtain the decline curve parameters. The parameters are plugged into Arps' model to estimate future performance. The distribution of the reserve estimates is determined accordingly. The generated synthetic realizations are assumed to be independent and identically distributed. However, bootstrapping is a sampling technique that requires no time dependency of the data; real production data follows an overall decline trend, which implies that the data points are not independent but are a sequence of successive observations.

The modified bootstrap method relies on decline curve analysis of the synthetic data sets. These synthetic data sets are created based on residuals obtained from production data and the best fit of any DCA model. Instead of sampling the actual residuals, Cheng and others (2010) created blocks of the residuals to stabilize the sampling data. To avoid the complications of the transient phase of the production data, their developed methodology consisted of a three stage backward approach. This approach eliminates the initial transient phase data to obtain better results. The first stage involves doing a DCA on the most recent 50% of the synthetic data generated by the aforementioned block residual approach. The second and third stages involve analyzing the most recent 30% and 20% of the data sets. The three stage DCA generates three different reserve distributions. Cheng and others (2010) stated that the minimum and maximum P90 and P10 from the three distributions can be considered as the actual P90 and P10, respectively. The actual P50 would be the mean of the three P50s of the three distributions. The approach was tested and calibrated on mature conventional wells having sufficient production history.

The major and most important assumption of Gong and others (2014) was that the logarithmic difference between the actual and estimated production history follows the standard normal distribution. Their likelihood function is based on this assumption and relies on the mean and standard deviation of the assumed normal distribution. The random walk algorithm is a sampling technique which is used for the MCMC sampling and is based on either accepting or rejecting the proposed DCA parameter set. The mean and standard deviation of the proposal distribution is incorporated into the likelihood function, which makes it challenging to compute. They used

flat/uniform prior distribution for the DCA parameters. Using the above defined functions, a Bayesian model was developed to quantify uncertainty.

As mentioned above, traditional Bayesian computation requires the computation of three important components, namely the likelihood function and prior and posterior distributions. Although the MCMC methodology is well calibrated, the likelihood computation becomes complex with a short production history (Gong et al., 2014). Therefore, we propose another way to quantify uncertainty from production data. This method integrates Approximate Bayesian Computation (ABC) methodology with rejection sampling. ABC methodology does not require the estimation of the likelihood and greatly simplifies the procedure. The concept behind ABC likelihood-free approximation is that the likelihood function is replaced with an approximation that is easier to compute (Turner and Zandt, 2012).

4.3 Approximate Bayesian Computation (ABC) methodology

In our proposed method, we approximate the posterior distribution by substituting different values of the decline equation parameters into a DCA model and generating a large number of production profiles. We will use Arps' equation to illustrate the process; however, the same approach can be used with any deterministic DCA model (as we will show with the LGA model later). The prior distributions for parameters b, D_i, and q_i are uniform distributions $0 \le b \le 3$, $0 < D_i \le 10$, and $0 < q_i \le 10000$ respectively. The likelihood function is approximated by the distance between the summary statistic of the simulated and the observed data sets. We call this $\rho(X, Y)$, where X is the actual production data, Y is the synthetic production data, and ρ is the distance function. In other words, it is the difference between the standard deviation of the actual production data and that of the computed production data from the decline curve model. The posterior distribution is the distribution of the DCA parameters after all the available production history has been taken into account and is computed using Bayes' theorem (Equation 1). However, the integral in the denominator of Bayes' theorem is difficult to compute analytically and therefore the posterior is numerically approximated with the rejection sampling algorithm.

Figure 4.1 explains the entire workflow for one simulation cycle, which starts by substituting random parameter values generated by a random number generator into Arps' model. This

generates a large amount of synthetic production data. The method thereafter replaces the likelihood with an approximation which is easier to calculate the distance $\rho(X,Y)$ between the summary statistics of the simulated and observed production datasets. Based on an optimum likelihood threshold value (ε), the decision is made to accept or discard the simulated production data. For small values of ε, approximately 10%, the posterior can be approximated by $\pi(\theta|\rho(X,Y) \leq \varepsilon)$. The resulting accepted data sets are used to approximate the posterior. The 10th, 50th, and 90th percentiles of the cumulative production are computed at 10-month increments, and at each time step, a distribution of the cumulative production is obtained. The 10th, 50th, and 90th percentiles of these distributions provide the P90, P50, and P10 estimates for reserves, respectively.

To avoid unreasonable solutions, the parameters of Arps' model are constrained as $0 \leq b \leq 3$, $0 < D_i \leq 10$, and $0 < q_i \leq 10000$. The constraints are the subsets of the parameter ranges for Arps' model (Kanfar and Wattenbarger, 2012). Accordingly, the constraints defined above serve as the minimum and maximum values (end points) of the uniform prior distributions that define the parameters of Arps' equation. Therefore, to estimate the posterior distribution, a set of random parameter values is sampled from their respective prior distributions to simulate a production data set.

To illustrate the procedure, suppose we generate 10,000 sets of DCA parameter values. We then store the parameter sets in a 10,000×3 matrix where each row corresponds to the parameter set to be used in a simulation run and each column corresponds to Arps' DCA parameters (b, D_i, and q_i). By substituting each row of this matrix into Arps' model, we generate 10,000 synthetic production data sets. For each synthetic production data set, we have a set of three summary statistics, namely the mean, standard deviation, and median absolute deviation. We also store these summary statistics in a 10,000×3 matrix. Finally, the equivalent three summary statistics for the actual production data are stored in vector form. When the ABC simulation is run, the rejection sampling algorithm compares each row of the simulated summary statistic matrix with the actual production summary statistic. If the difference between the simulated and actual summary statistic is less than the 10% (threshold) of the actual summary statistic for all the columns in a given row, then the algorithm accepts the simulated production data. All the simulations that do not meet this requirement are rejected. The distribution of the accepted parameter values is an approximation of

the posterior distribution. This workflow is coded in the R programming language (R Project for Statistical Computing).

The choice of prior distribution, whether informative or non-informative (uniform prior), has negligible effects on the posterior whenever the posterior is a subset of the assumed prior distribution. The prior is merely the initial distribution from which samples are drawn to compute the approximate likelihood function. For this reason, the uniform prior does not affect the posterior significantly.

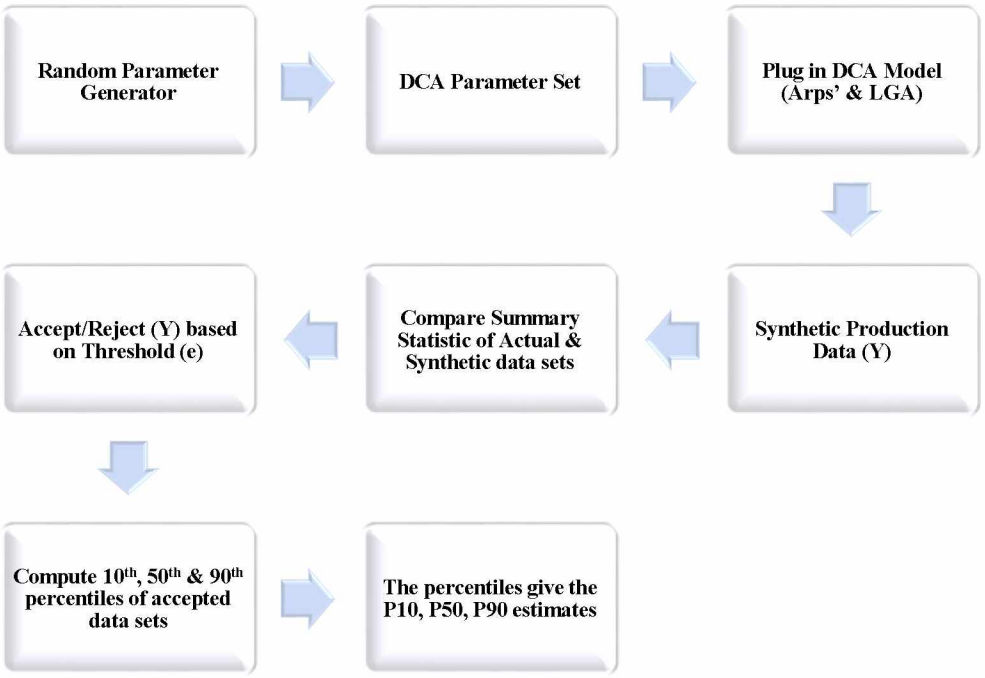

Figure 4.1: Flow diagram for Approximate Bayesian Computation

4.4 Validation of the methodology

Figure 4.2 shows a semi-log rate vs. time plot for an example well with MCMC P10-P50-P90 bounds shown in red. This plot is from Gong and others' 2014 paper. Using the ABC methodology along with Arps' model, as explained above, uncertainty was quantified using the same data set (Figure 4.3). Again, the bounds in red represent the reproduced MCMC bounds. The bounds in green represent the ABC P10-P50-P90 bounds. The first observation is that both methods bracket the production history in their respective P90 to P10 ranges. However, the ABC interval is

narrower than the MCMC interval. Assuming both methods quantify uncertainty adequately, then a tighter range is more desirable.

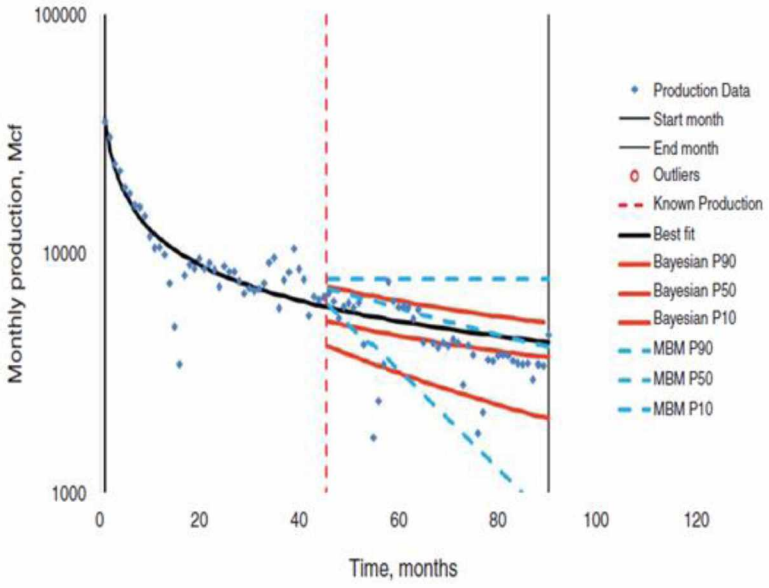

Figure 4.2: MCMC probabilistic forecasts (Gong et al., 2014)

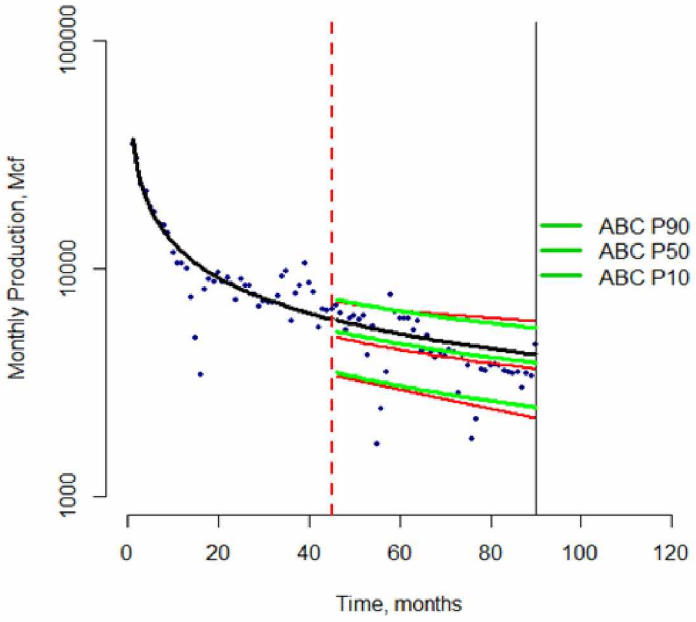

Figure 4.3: Comparison of ABC and MCMC forecasts

4.5 Results and Discussion

4.5.1 Example case study to illustrate the process

Hindcasting is a technique where some portion of the production history is used to history match and the remaining part is used for prediction/forecasting. Hindcasting was used to illustrate the effect of increasing production history on the P90-P10 interval when the approximate Bayesian model is applied to the data. Figure 4.4 shows semi-log rate-time plots for an example well from the Barnett Shale in Johnson County. The amount of production history used for computation was increased from 30 to 70 months (increments of 10 months) as shown in Figure 4.4. For all the cases, the remaining production history was used to check the accuracy of the methods' predictions.

We observed that the P90-P10 intervals tighten with increasing production history as expected. Figure 4.5 shows the probabilistic hindcasts for cumulative production (G_p) of the same well. In this hindcast, the production history used for modeling was varied from 30 to 70 months. The results were then plotted against the number of months used for modeling. The highest estimate of cumulative production obtained by the hindcast was the P10 estimate, while the P90 estimate was the lowest. The true value for G_p was inside the P90-P10 interval for all the cases. The P50 estimate asymptotically approaches the true G_p value as more production data becomes available for modeling. Also, as expected, the uncertainty associated with the forecasts decreases with the use of more production data. This can be seen from the narrowing P90-P10 band (Figure 4.5).

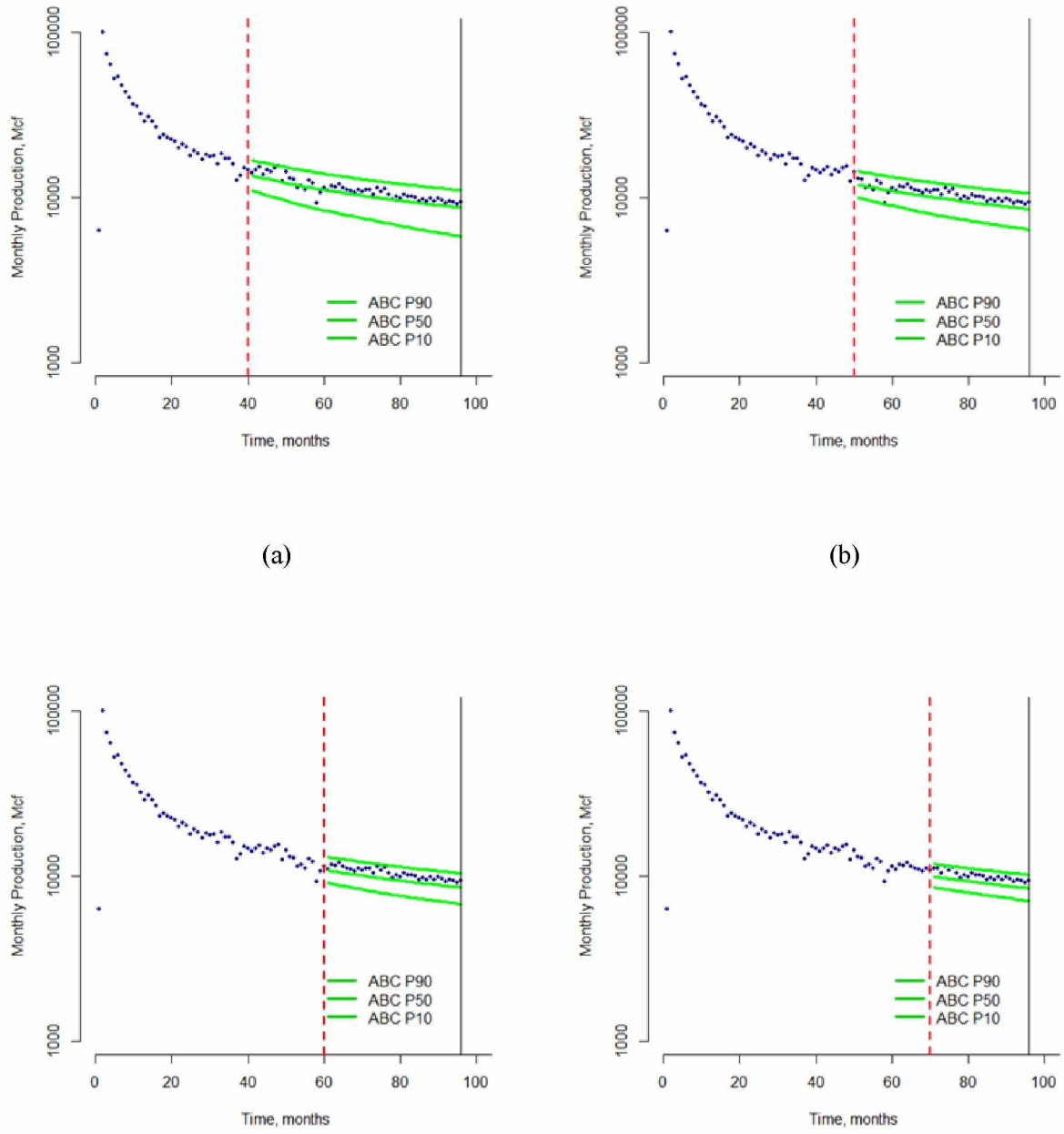

Figure 4.4: ABC probabilistic forecasts for an example well in Johnson County with increasing amounts of production history used for modeling a) 40 months, b) 50 months, c) 60 months, d) 70 months

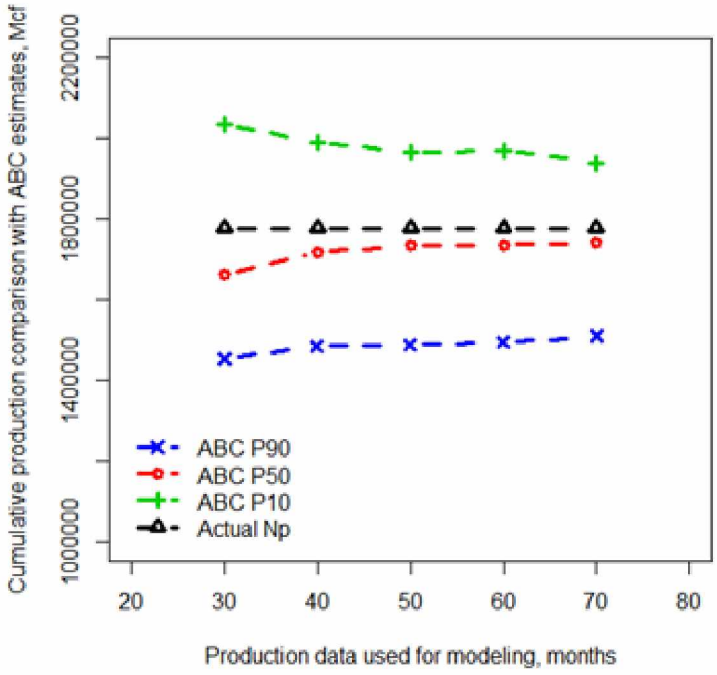

Figure 4.5: Uncertainty decreases with increasing production history

4.5.2 Application of methodology to groups of wells using Arps' model

21 oil wells from the Eagle Ford Shale in Karnes County with production lengths of 45 months were selected randomly. After shifting the initial maximum production of the individual wells to a common starting point, the production was averaged and used for the analysis. We did a similar analysis using 57 Barnett Shale gas wells from Johnson County. Both examples used Arps' equation as the DCA model.

Figure 4.6 shows that the ABC P90-P50-P10 average interval per well in Karnes County was 170-184-204 MSTB, while the true average cumulative production per well was 183 MSTB. Similarly, Figure 4.7 shows that the ABC P90-P50-P10 average cumulative production interval for wells in Johnson County was 1263-1410-1528 MMscf, while true average cumulative production per well was 1425 MMcf. These results imply that the ABC method brackets the true reserve adequately.

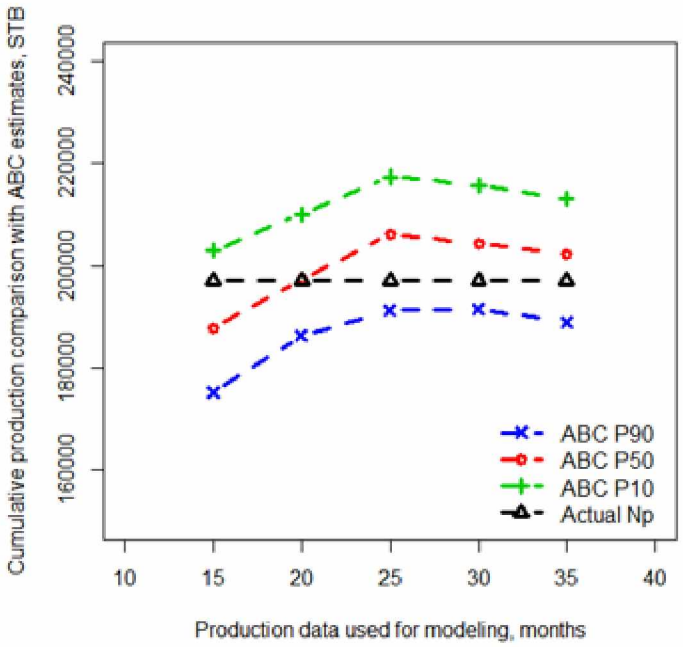

Figure 4.6: Average probabilistic hindcasts for cumulative production using Arps' model on data from wells in Karnes County

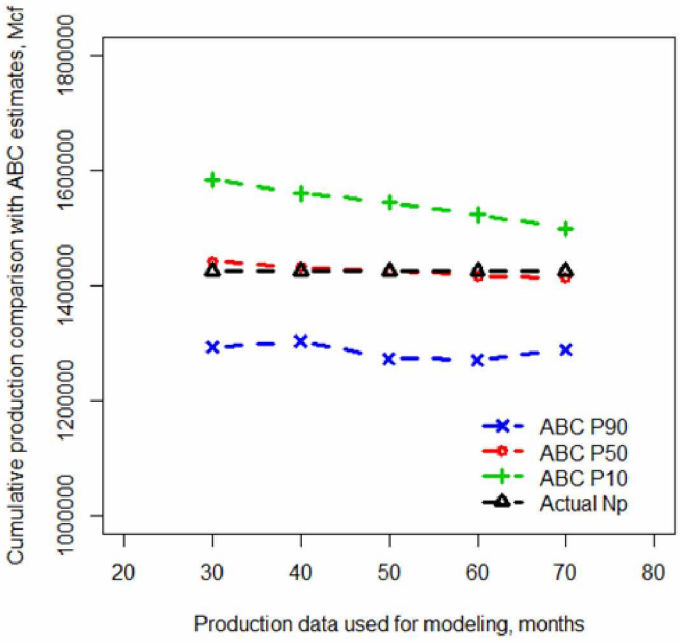

Figure 4.7: Average probabilistic hindcasts for cumulative production using Arps' model on data from wells in Johnson County

4.5.3 Application of methodology to a group of wells using the LGA model

Figure 4.6 shows that for short production histories, even though the P90-P10 bounds bracket the true reserves, the P50 estimate does not always asymptotically increase or decrease to the true cumulative production. This is probably because of the wells' limited production history. We replaced Arps' model with the LGA model in an attempt to improve the results. This is because in our previous work (Paryani et al., 2015), we observed that in wells with limited production histories, the LGA model provided better estimates of reserves. The prior distribution defined for the LGA-ABC approach was an uninformative uniform distribution. The bounds for the distribution and the parameters of the LGA model were constrained as $0 \leq K \leq 1000000$, $0 < n < 1$ and $0 < a \leq 500$ (Kanfar and Wattenbarger, 2012).

Figure 4.8 shows the results when the LGA model was used in conjunction with the ABC methodology. We saw that there was significant improvement in the trend of the P50 match with the true cumulative production estimate as a function of production history.

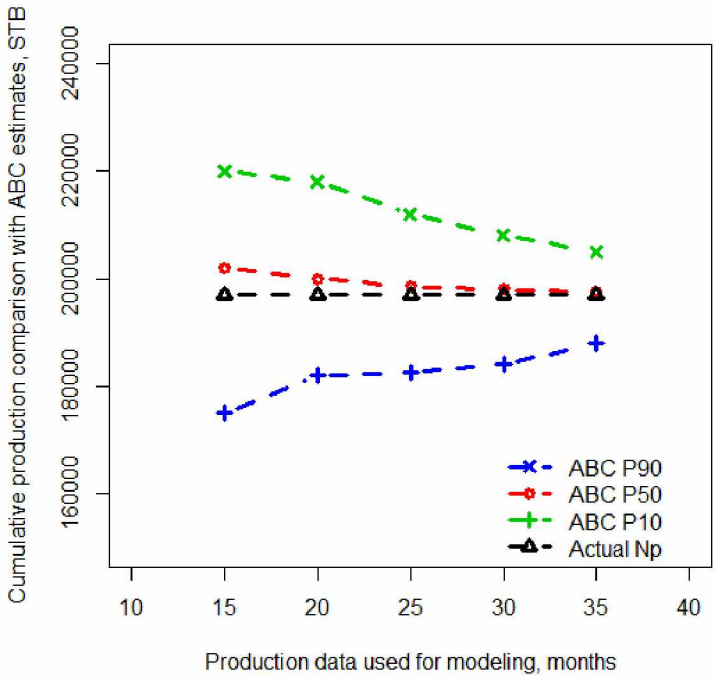

Figure 4.8: Average probabilistic hindcasts for cumulative production from Karnes County using ABC-LGA

4.5.4 Calibration test using data from 100 gas wells in the Barnett Shale

Narrow bounds are a necessary but not sufficient condition for assessing the reliability of a method. Therefore, in order to ensure this method is properly calibrated, the hindcasting technique was applied individually to 100 gas wells from the Barnett Shale with the production histories of 96-108 months (Table 4.1). Figure 4.9 is compares the true cumulative production and the estimated ABC P90-P50-P10 values at the end of the hindcast.

Table 4.1: Well statistics

Shale Play	County	Well Type	Number of Wells
Barnett	Johnson	Gas	57
Barnett	Denton	Gas	22
Barnett	McMullen	Gas	21

In Figure 4.9, the frequencies with which the true values exceed the ABC P90-P50-P10 values are recorded and plotted on the Y-axis. The number of months used for modeling is plotted on the X-axis. The P90-P10 interval brackets the true value at the end of hindcast approximately 80% of the time when a production history of 40 months or more was used for modeling. The definition of the P10, P50, and P90 estimates states that the probability of obtaining true values greater than the estimates is 10%, 50%, and 90%, respectively. This implies that if the frequencies for true values greater than ABC estimates are at least 10% for P10, 50% for P50, and 90% for P90, respectively, the methodology is well calibrated. As shown in Figure 4.9, this condition is approximately satisfied for the hundred wells analyzed when 30-50 months of production history was used for modeling. When 60-70 months of production history was used for modeling, the calibration condition was very satisfied, giving precise confidence intervals of 80%. Therefore, estimates of cumulative production from the ABC methodology are well calibrated.

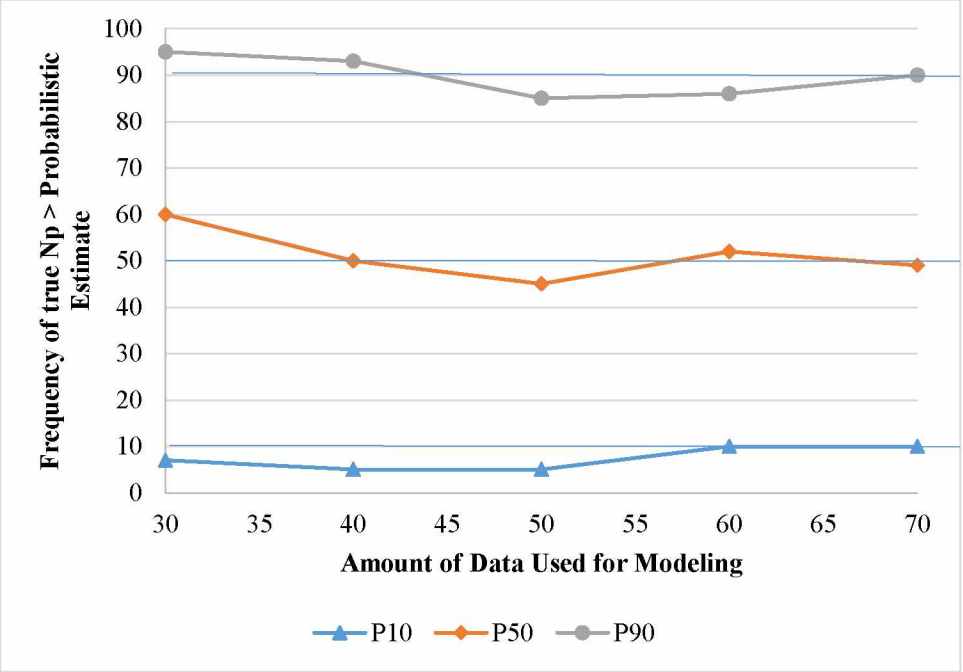

Figure 4.9: Validation results showing a good match of true and estimated cumulative production in terms of honoring the definitions of P90-P50-P10 forecasts

4.6 Case study: comparison of results with reserve estimates obtained from frac design software

The results of any model depend on the completeness and quality of the input data. In this work, different well logs, 3D well surveys, and treating pressures were digitized from various publications (Suliman et al., 2013; Diakhate et al., 2015; Jaripatke and Pandya, 2013). This was to ensure accurate reservoir characterization and for history matching purposes. To illustrate the process, the Eagle Ford well design is implemented in GOHFER, but the methodology could be easily applied with FRACPRO, StimPlan, or any other frac design software.

To build the base case model, gamma ray, resistivity, effective porosity, and total organic content (TOC) logs were input into the frac design software. Other data such as formation porosity and permeability, rock mechanical properties, fracturing fluid and proppant properties, and the proposed pumping schedule were added. The available effective porosity and gamma ray logs were used to estimate the average porosity and permeability of the Eagle Ford reservoir. The rock mechanical properties play an important role in selection of the fracturing fluid/proppant and the pumping schedule for the stimulation treatment, the most important ones being Young's Modulus and Poisson's Ratio. Since the compressional travel time (DTC) log was unavailable, the frac design software estimated that variable using surrogate correlation based DTC logs derived from the gamma ray, resistivity, and average porosity logs. The dynamic Young's Modulus (YM) was computed using the aforementioned DTC correlation. The best prediction of the static YM was obtained from the bulk density and the dynamic YM. However, as the actual bulk density log was unavailable, it was itself approximated using the dynamic YM correlation. Similarly, Poisson's Ratio (PR) was computed via synthetic correlations using the gamma ray, resistivity, and DTC logs. The value of Poisson's Ratio used in this study was between 0.28 and 0.3.

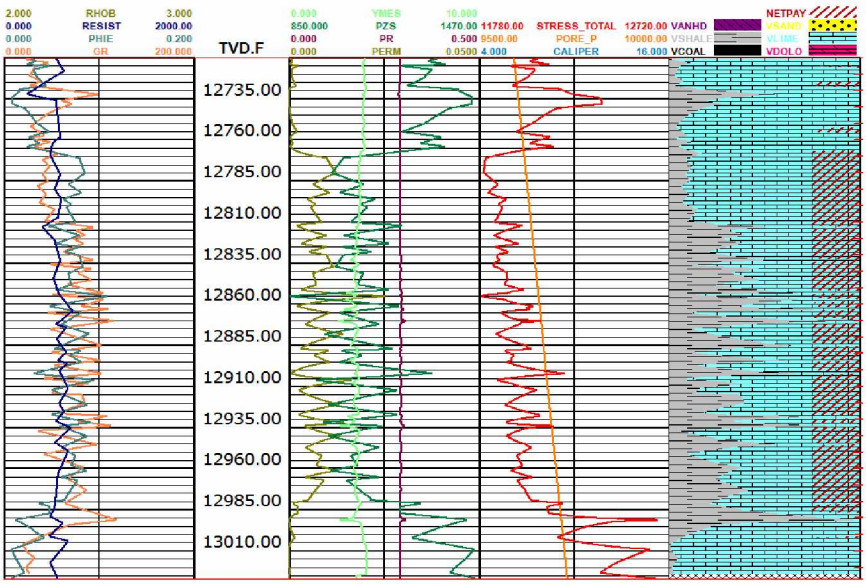

Figure 4.10: Input and output logs used to model the Eagle Ford well (Ouenes et al., 2015)

The minimum horizontal stress component controls the direction and extent of the hydraulic fracture propagation and is one of the most important parameters to characterize accurately. The azimuth of the horizontal Eagle Ford well was 153 degrees (Diakhate et al., 2015). Accordingly, an azimuth of maximum horizontal stress of 63 degrees was chosen to generate transverse multiple fractures. A pore pressure offset of approximately 4000 psi was chosen to match the published reservoir pressure of 10,000 psi (Diakhate et al., 2015). The closure stress/minimum horizontal stress was computed based on the above input and curves using the stress equation available in the frac design software. Figure 4.10 shows the input and output logs along with the vertical variations.

A preliminary simulation was done in order to validate the correlations used for building the data set, which reproduced the typical fracture half-lengths published for the Eagle Ford well under consideration (Suliman et al., 2013). The most efficient and frequently used fluid is slickwater, due to its availability and relatively low cost. Slickwater was used as the completion design fluid for the preliminary base case, as it was in the early Eagle Ford wells (Jaripatke and Pandya, 2013). This resulted in a symmetric bi-wing fracture geometry. In order to improve the fracture conductivity in shale reservoirs, a hybrid fluid system was used to enhance the proppant carrying capacity of the fracturing fluid. In this hybrid system, slickwater was typically replaced with linear gel to improve the proppant carrying capacity when needed. Carboprop 30/60 and 20/40 were used as proppants.

Figure 4.11 shows the planar grid with total stress distribution, the well survey, and the nine frac stages along the horizontal section. The effective treatment diameter is 4.548 inches from the surface to a measured depth of 17,155 feet and a TVD of 12,969 feet. The perforated intervals consist of nine stages with four clusters per stage, 70 feet apart with eight perforations per cluster, 0.38 inches diameter and 3 feet apart.

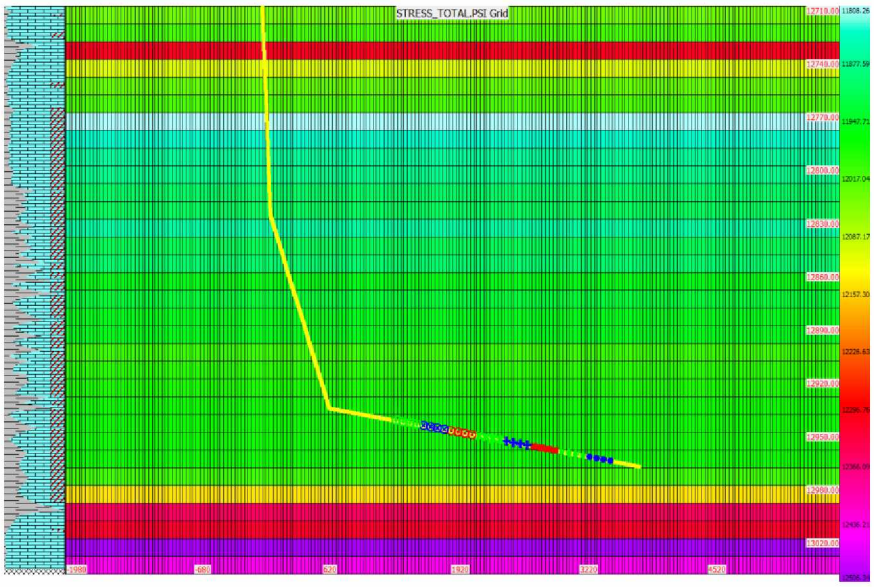

Figure 4.11: Total stress distribution (Ouenes et al., 2015)

The frac design software creates a transverse planar grid for each cluster in a stage and computes the fracture geometry accordingly. Figure 4.12 shows the modeled fracture geometry of one of the stages for the base case. The model predicts a proppant cutoff length of approximately 180 feet and propped lengths extending up to 480 feet, which is in good agreement with the microseismic and analytical results from Suliman and others (2013). Figure 4.13 shows the side and top view of the horizontal well along with multiple transverse fractures with symmetric bi-wing geometries.

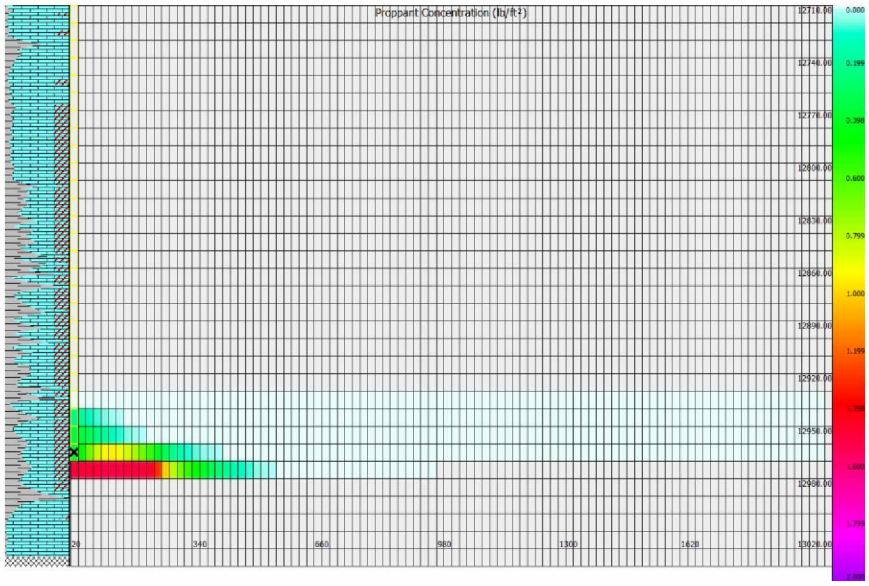

Figure 4.12: Duplicating the initial modeled fracture geometry (bi-wing) (Ouenes et al., 2015)

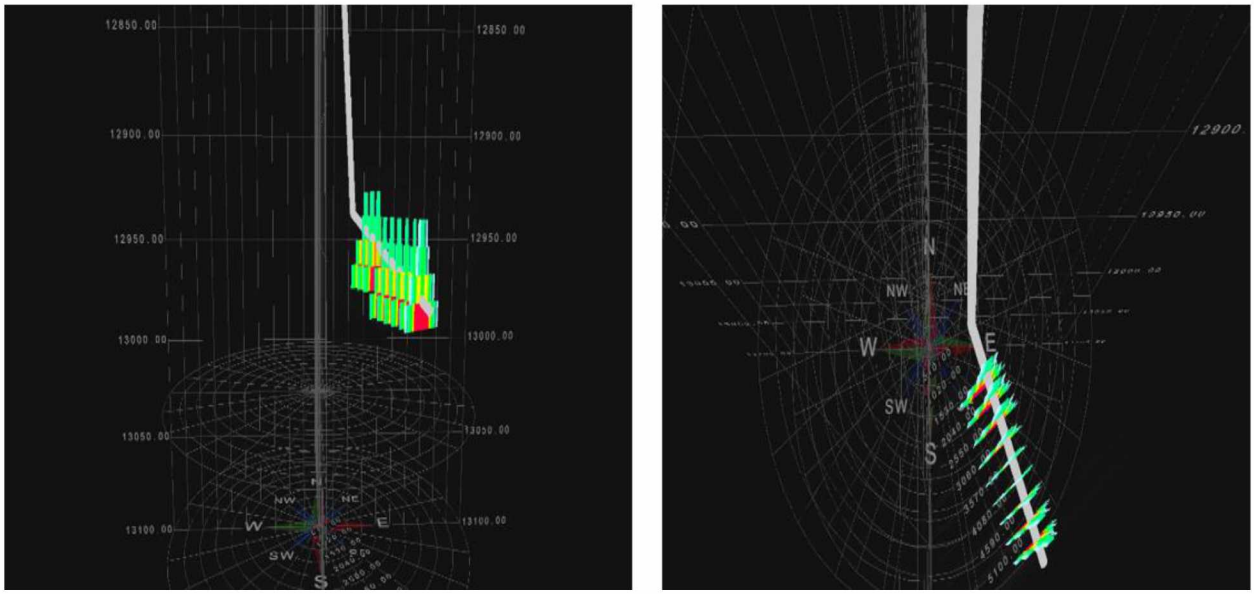

Figure 4.13: Side (left) and top view (right) for 9 stages of the base case showing the symmetric frac stages (Ouenes et al., 2015)

Figure 4.14 shows the simulated surface and bottomhole treating pressures and the simulated instantaneous shut in pressure (ISIP) of approximately 7000 psi for a typical base case frac stage. The figure shows a good match of the simulated and the actual treating pressures along with good agreement of the simulated and the actual ISIP of 7000 psi (Diakhate et al., 2015).

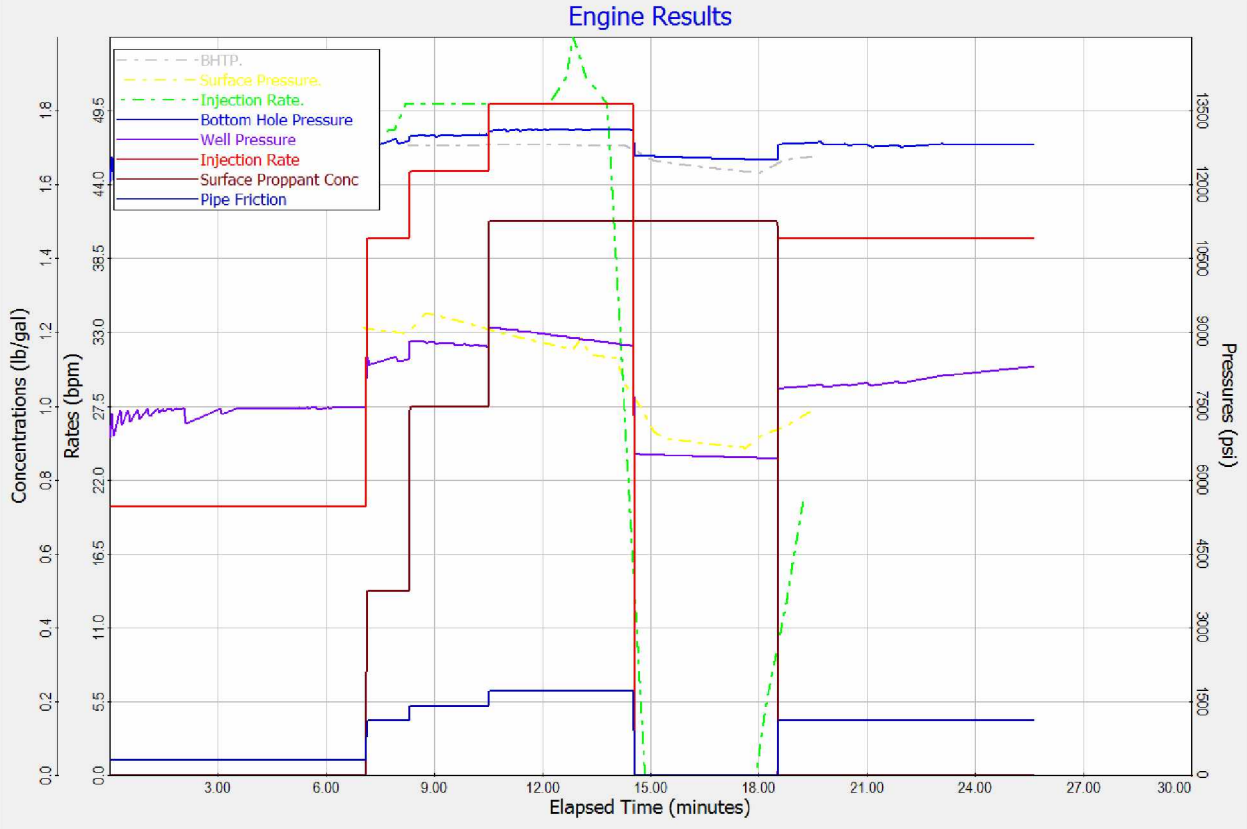

Figure 4.14: Simulated (continuous lines) and actual pressure match (dashed lines) (Ouenes et al., 2015)

To compare the simulator and ABC results, the gas production data of this well was digitized. Figure 4.15 shows the actual gas rate and cumulative history for the Eagle Ford well. Figure 4.16 is the digitized rate history. The blue line shows the expected simulated rates, which are based on the fracture model output, the assumed and computed reservoir properties, and the generated stimulated reservoir volume of the fractures. The green lines in Figure 4.16 show the ABC estimates where only 500 days of data were used for modeling. Clearly, the P50 estimate matches the simulation forecast.

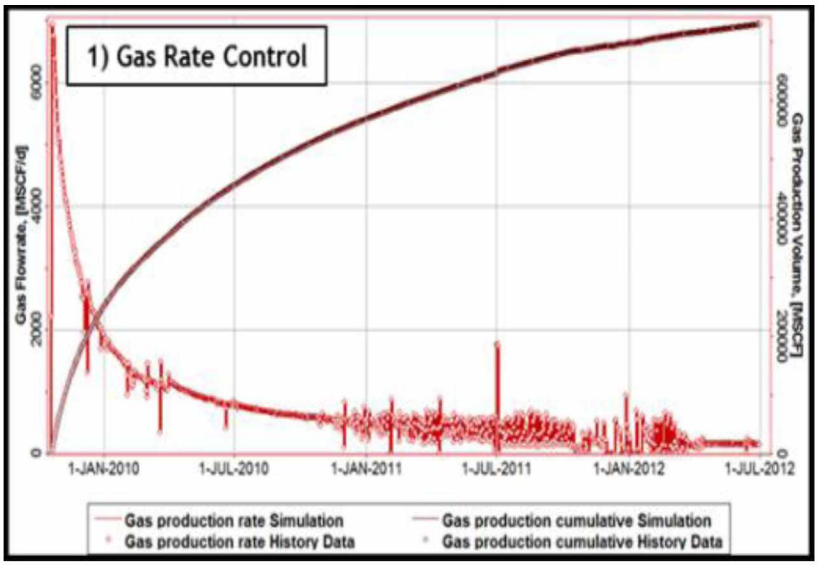

Figure 4.15: Gas rate history (Suliman et al., 2013)

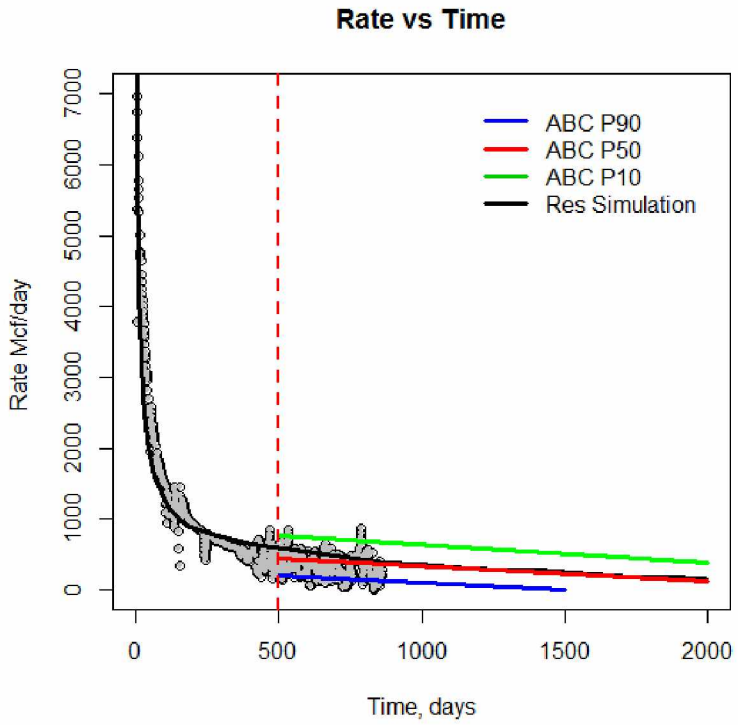

Figure 4.16: Comparison between ABC and simulation forecasts

Chapter 5. Conclusions and Recommendations

This study highlights some of the pitfalls of using decline curve analysis (DCA) models developed for conventional reservoirs to predict future production of shale wells. As seen in the first part of this study (Chapter 2), the actual production profiles of wells in the Eagle Ford Shale are often erratic; it is difficult to distinguish a reasonable decline trend without filtering out off-trend data. This difficulty may affect the results of the DCA; filtering may be biased and introduce errors in future estimates. However, the smoothed data can be fitted well with most of the models.

Based on decline analysis of 100 oil wells from eight different counties in the Eagle Ford shale, Arps' exponential analysis is a conservative approach for estimating reserves and forecasting future performance. However, Arps' exponential decline relation rarely applies at $R^2 \geq 0.95$. Arps' hyperbolic approach consistently provided high estimates, and may be described as the optimistic approach for generating future production predictions. Arps' hyperbolic method proved unsuccessful in correctly estimating reserves and generating future production trends because of the unusually high Arps' decline exponent b. Forecasting transient production with Arps hyperbolic equation with $b > 1$ can lead to a severe overestimation of expected ultimate recovery (EUR) and remaining reserves.

Overall, the logistic growth analysis (LGA) model fits 81% of the wells' past production rates and cumulative production. The lack of a good history match with the remaining wells may be due to the absence of long production histories. The LGA model gives reasonable EUR estimates compared with those of Arps' models.

Duong's model fits the production rate and cumulative production data of about 51% of the Eagle Ford wells. Duong's model performed well when the production history was at least 20–24 months with minimum noise. For a few cases, even when the data was smoothed, Duong's model did not match the production history well. Sometimes the results indicated extremely high reserve estimates (as with Arps' hyperbolic model), or extremely low reserve estimates (as with Arps' exponential model), suggesting that Duong's model needs further modifications in order to be applicable to shale wells with short production histories.

As the power law exponential (PLE) originates from the exponential family of curves, it behaved similarly to Arps' exponential model. The PLE consistently predicted the lowest forecasts of all the models; therefore, it is the most conservative method for production forecasting and reserve estimation. Based on $R^2 \geq 0.95$, the PLE fits the production rates of 67% of the wells.

These results suggest that the LGA, the PLE, and Duong's models overcome the limitations of Arps' models up to a certain point when modeling past production of a shale well, with the logistic growth analysis being the most successful. However, there is still scope for a better model in terms of consistency in fitting a well's past production.

The results of this study suggest that applying Arps' hyperbolic model to shale oil wells will consistently provide overly optimistic estimates of reserves and predict a long remaining life of shale wells. The LGA, PLE, and Duong's models overcome the limitations of Arps' models to varying degrees. PLE consistently predicted the lowest EUR of all the models, with the most conservative production forecasting and reserves estimation. Duong's model performed best when a longer and less noisy production history was available. However, erratic expected ultimate recovery (EUR) predictions indicate that Duong's model needs further improvements. The LGA model gives reasonable EUR estimates compared to Arps' model. Overall, the LGA model appears to be the most effective at history matching past production and predicting finite reasonable EUR.

Even though the normalized cumulative-time residual function gave a good history match, it resulted in unrealistic values. Arps' normalized and Arps' logarithmic residual functions reduce the fitting parameters q_i, D_i, and b for Arps' hyperbolic model by ranges of 15-79%, 31-86%, and 20-35%, respectively. Using the logarithmic and normalized rate-time residuals increases the tendency of Arps' model to have bounded estimates of wells' remaining reserves and life by approximately 87.5% and 50%, respectively. Thus using normalized and logarithmic rate-time residuals overcomes the limitations, and improves the accuracy, of Arps' model in the case of unconventional reservoirs. The proposed residual functions can be used to provide multiple estimations of remaining reserves and/or remaining life using any of the above decline models. They also allow for the most recent production data to be weighted more heavily, thereby ensuring that the fitted parameters reflect the current flow regime in the drainage area of the wells.

In part 2 of this study, a methodology was developed that integrated DCA models with an approximate Bayesian computation (ABC) method in order to quantify the uncertainty associated with the DCA models. The method used production data from 100 hydraulically fractured horizontal gas wells from the Barnett Shale and 21 hydraulically fractured oil wells from the Eagle Ford Shale. This ABC methodology combined with rejection sampling provides a likelihood-free procedure that not only simplifies the computational requirements significantly, but also quantifies reserves uncertainty in unconventional plays quickly, consistently, and efficiently, even with limited production histories. The ABC methodology can be used with Arps' model, LGA, or any other deterministic DCA model. Regardless of which DCA model is used, the uncertainty in cumulative production decreases as the amount of production history used for modeling increases.

The ABC technique is computationally faster than the likelihood-based numerical approximation method because the likelihood is not evaluated directly, but is replaced with an approximation that is usually easier to compute. While uncertainty will always be present in any production forecast and/or reserves estimation and will likely be quite large early in the producing life of a well or producing field, the reliable assessment of uncertainty enables better assessment of upside and downside potential, as well as better assessment of the expected value of the reserve estimates. The ABC method provides a quick way to constrain reserve estimates based on limited production data.

The potential limitations of this work are: a) the methodology is tested using hindcasts for up to 108 months only--we do not know how it will perform outside this time range, as not much data is available; b) the method relies solely on the integrated deterministic model and Bayesian inference--it does not consider other types of information.

The advantage of performing Probabilistic DCA is that it relies solely on the analysis of production data. However, to decrease the uncertainty further and provide more accurate forecasts and reserve estimates, we recommended incorporating other important factors such as the drainage area, stimulated reservoir volume, and reservoir rock and fluid properties, among others. We also recommended updating the ABC reserve estimates with information from volumetric data and any additional production data. To make the proposed ABC methodology more robust, we suggest

taking advantage of all the known information regarding the reservoir in order to reduce uncertainty.

References

Agrawal, A., Wei, Y., & Holditch, S. 2012. A Technical and Economic Study of Completion Techniques in Five Emerging US Gas Shales: A Woodford Shale Example. *SPE Drilling & Completion*. **27** (01): 39 – 49 SPE-135396-PA http://dx.doi.org/10.2118/135396-PA

Arps, J. J. 1945. Analysis of Decline Curves. *Transactions of the AIME* **160** (01): 228 – 247 SPE-945228-G. http://dx.doi.org/10.2118/945228-G

Chaudhary, A. S., Ehlig-Economides, C. A., & Wattenbarger, R. A. 2011. Shale Oil Production Performance from a Stimulated Reservoir Volume. Presented at the SPE Annual Technical Conference and Exhibition, 30 October-2 November, Denver, Colorado, USA. SPE-147596-MS. http://dx.doi.org/10.2118/147596-MS

Cheng, Y., Wang, Y., McVay, D., & Lee, W. J. 2010. Practical Application of a Probabilistic Approach to Estimate Reserves Using Production Decline Data. *SPE Economics & Management* **2** (1): 19-31. http://dx.doi.org/10.2118/95974-PA

Clark, A. J., Lake, L. W., & Patzek, T. W. 2011. Production Forecasting with Logistic Growth Models. Presented at the SPE Annual Technical Conference and Exhibition, 30 October-2 November, Denver, Colorado, USA. SPE 144790-MS http://dx.doi.org/10.2118/144790-MS

Diakhate, M., Gazawi, A., Barree, R. D., Cossio, M., Tinnin, B., McDonald, B., & Barzola, G. (2015, February 3). Refracturing on Horizontal Wells in the Eagle Ford Shale in South Texas - One Operator's Perspective. Society of Petroleum Engineers. doi:10.2118/173333-MS

Dossary, M., & McVay, D. A. 2012. The Value of Assessing Uncertainty. Presented at the SPE Annual Technical Conference and Exhibition, 8-10 October, San Antonio. SPE-160189-MS http://dx.doi.org/10.2118/160189-MS

DuBose, K. E. 22 June 2011. Web. 25 Oct. 2015. Eagle Ford Shale Map. Digital image. www.eaglefordshale.com. <http://eaglefordshale.com/maps/attachment/eagle-ford-shale-map-800x614-2/>.

Duong, A. N. 2011. Rate-Decline Analysis for Fracture-Dominated Shale Reservoirs. *SPE Reservoir Evaluation & Engineering* **14** (03): 377 - 387 SPE-137748-PA. http://dx.doi.org/10.2118/137748-PA

Gong, X., Gonzalez, R., McVay, D. A., & Hart, J. D. 2014. Bayesian Probabilistic Decline-Curve Analysis Reliably Quantifies Uncertainty in Shale-Well-Production Forecasts. *SPE Journal*. **19** (06): 1,047 - 1,057. SPE-147588-PA. http://dx.doi.org/10.2118/147588-PA

Ilk, D., Rushing, J. A., Perego, A. D., & Blasingame, T. A. (2008, January 1). Exponential vs. Hyperbolic Decline in Tight Gas Sands: Understanding the Origin and Implications for Reserve Estimates Using Arps Decline Curves. Presented at the SPE Annual Technical Conference and Exhibition, 21-24 September, Denver, Colorado, USA. SPE-116731-MS. http://dx.doi.org/10.2118/116731-MS

Jaripatke, O., & Pandya, N. (2013, August 12). Eagle Ford Completions Optimization - An Operator's Approach. Society of Petroleum Engineers. doi:10.1190/URTEC2013-072

Jochen, V. A., & Spivey, J. P. 1996. Probabilistic Reserves Estimation Using Decline Curve Analysis with the Bootstrap Method. Presented at the SPE Annual Technical Conference and Exhibition, 6-9 October, Denver, Colorado. SPE-36633-MS http://dx.doi.org/10.2118/36633-MS

Kanfar, M., & Wattenbarger, R. 2012. Comparison of Empirical Decline Curve Methods for Shale Wells. Presented at the SPE Canadian Unconventional Resources Conference, 30 October-1 November, Calgary, Alberta, Canada. SPE 162648-MS http://dx.doi.org/10.2118/162648-MS

Kruschke, J. K. 2011. *Doing Bayesian Data Analysis: A Tutorial with R and BUGS*. Burlington, MA: Academic Press.

Lee, W. J., & Sidle, R. 2010. Gas-Reserves Estimation in Resource Plays. SPE Economics & Management **2** (02): 86 – 91 SPE-130102-PA. http://dx.doi.org/10.2118/130102-PA

McNeil, R., Jeje, O., & Renaud, A. 2009. Application of the Power Law Loss-Ratio Method of Decline Analysis. Presented at the Canadian International Petroleum Conference, 16-18 June, Calgary, Alberta. PETSOC-2009-159. http://dx.doi.org/10.2118/2009-159

Ouenes, A. Bachir, M. Paryani, & R. Smaoui. 2015. Estimation of Propped Volume Permeability Using Strain from Geomechanical Modeling of Interacting Hydraulic and Natural Fractures – Application to the Eagle Ford. Presented at the SPE Unconventional Resources Conferences, 20-22 October, Calgary, Canada. SPE-175971-MS. http://dx.doi.org/10.2118/175971-MS

Paryani, M., Ahmadi, M., Awoleke, O. & Hanks, C. 2015. Influence of Residual Function Form on the Performance of Decline Curve Analysis Models for Shale Oil Wells. Manuscript submitted for peer review in the *SPE Res Eval & Eng* Journal

Suliman, B., Meek, R., Hull, R., Bello, H., Portis, D., & Richmond, P. 2013. Variable Stimulated Reservoir Volume (SRV) Simulation: Eagle Ford Shale Case Study. Presented at the SPE Unconventional Resources Technology Conference, 12-14 August, Denver, Colorado, USA. SPE-168832-MS http://dx.doi.org/10.1190/URTEC2013-057

Tsoularis, A. & J. Wallace, 2001. Analysis of logistic growth models. Mathematical Biosciences **179** (1): 21-55 ISSN 0025-5564. http://dx.doi.org/10.1016/S0025-5564(02)00096-2.

Turner, B., Zandt, T. 2012. A tutorial on approximate Bayesian computation. *Journal of Mathematical Psychology*. **56** (2): 69-85, ISSN 0022-2496. http://dx.doi.org/10.1016/j.jmp.2012.02.005.

Urbancic, T. & Baig, A. 2004. Enhancing Recovery in Shales Through Stimulation of Pre-Existing Fracture Networks. Presented at the SPE Hydraulic Technology Conference, Woodlands, Texas, USA, 4-6 February. SPE-168591-MS. http://dx.doi.org/10.2118/168591-MS

Appendix – Abbreviations and Nomenclature

List of Abbreviations

Abbreviation	Full Meaning
DCA	Decline Curve Analysis
LGA	Logistic Growth Analysis
LGA EUR	Estimated Ultimate Recovery from Logistic Growth Analysis
PLE	Power Law Exponential
SRV	Stimulated Reservoir Volume
MSTB	Thousand Stock Tank Barrels
ABC	Approximate Bayesian Computation
MCMC	Markov Chain Monte Carlo
EUR	Estimated Ultimate Recovery
STB	Stock Tank Barrels
CDF	Cumulative Distribution Function
MBM	Modified Bootstrap Method

MMcf	Million Cubic Feet
TOC	Total Organic Content
DTC	Compressional Travel Time
YM	Young's Modulus
PR	Poisson's Ratio
TVD	True Vertical Depth
ISIP	Instantaneous Shut In Pressure

List of Symbols

Symbols	Meaning
q	Production rate, volume/time
t	Time
b	Decline exponent $0 \leq b \leq 1$
$q(t)$	Production rate at time t, volume/time
q_i	Initial production rate, volume/time
Di	Initial decline constant, 1/time
$Q(t)$	Cumulative production, volume
K	Carrying capacity, STB
a''	Constant of t^n, time
n	Exponential parameter
a	Intercept constant, 1/time
m	Slope
q_1	Oil rate at day

q_∞	Oil rate at infinite time
$t(a,m)$	Time function
$\hat{q}_i$	Rate at t=0, volume/time
D_1	Decline constant after at time =1, 1/time
D_∞	Decline constant at infinite time, 1/time
$\hat{D}_i$	Decline constant $=\frac{D_1}{n}$, 1/time
n'	Time exponent
$q(t)_i$	Production rate of month i, STB/day
t_i	Number of days in month i, days
x	The month number when rate is 2 STB/day
θ_j	DCA parameters
y	Production data
$\pi(\theta_j)$	Prior distribution
$f(y\|\theta_j)$	Likelihood function

$\pi(\theta_j \mid y)$	Posterior distribution